HYPERSONIC LAMINAR WAKES AND TRANSITION STUDIES
(Tasks 3.1 and 3.5 -- REST Project)

Prepared by

A. J. Pallone
J. I. Erdos
J. Eckerman

RESEARCH AND ADVANCED DEVELOPMENT DIVISION
AVCO CORPORATION
Wilmington, Massachusetts

Technical Memorandum
RAD-TM-63-33, Rev. 1
Contract AF04(694)-239

THIS REPORT WAS PREPARED IN ACCORDANCE WITH AIR FORCE CONTRACT AF04(694)-239. IT IS SUBMITTED IN PARTIAL FULFILLMENT OF THE CONTRACT AND IN ACCORDANCE WITH AFBM EXHIBIT 58-1 (PARAGRAPH 4.2.1).

25 November 1963

Prepared for

AIR FORCE BALLISTIC SYSTEMS DIVISION
AIR FORCE SYSTEMS COMMAND
UNITED STATES AIR FORCE
Norton Air Force Base, California

AFBSD-

This document consists of 70 pages,
173 copies, Series A

HYPERSONIC LAMINAR WAKES AND TRANSITION STUDIES (Tasks 3.1 and 3.5 -- REST Project)

Prepared by

A. J. Pallone
J. I. Erdos
J. Eckerman

RESEARCH AND ADVANCED DEVELOPMENT DIVISION
AVCO CORPORATION
Wilmington, Massachusetts

Technical Memorandum
RAD-TM-63-33, Rev. 1
Contract AF04(694)-239

THIS REPORT WAS PREPARED IN ACCORDANCE WITH AIR FORCE CONTRACT AF04(694)-239. IT IS SUBMITTED IN PARTIAL FULFILLMENT OF THE CONTRACT AND IN ACCORDANCE WITH AFBM EXHIBIT 58-1 (PARAGRAPH 4.2.1).

25 November 1963

APPROVED

A. J. Pallone, Project Engineer
Flow Field Analyses

J. A. Luceri, Manager
REST Project Office

CLEARED FOR PUBLIC RELEASE BY AIR FORCE BALLISTIC SYSTEMS DIVISION, BSES, LETTER OF 23 OCTOBER 1963.

Prepared for

AIR FORCE BALLISTIC SYSTEMS DIVISION
AIR FORCE SYSTEMS COMMAND
UNITED STATES AIR FORCE
Norton Air Force Base, California

ABSTRACT

This report presents the results of theoretical and experimental investigations of the flow in the wake of hypersonic vehicles. Nonsimilar solutions of the equations governing the "far wake" are obtained and contrasted with similar solutions and with solutions involving the Karman-Pohlhausen approach. Numerical examples of the flow field in the wake of ballistic-range and wind-tunnel models and of a flight-size vehicle are presented.

A series of ballistic-range experiments with conical models of 10, 15, and 27-1/2-degree half-angles are described. The model velocity ranges between 4,000 and 17,000 ft/sec with range pressures varying from 15 to 380 mmHg in air. The experimental data is discussed in detail, and the analysis is used to compute and correlate appropriate transition parameters.

Based on the correlation, predictions of the location of transition in the wake of a 12-degree half-angle cone at 22,000 ft/sec are made for the altitude range from 200,000 to 100,000 feet. For example, transition is placed at approximately 250, 100, and 20 feet from the apex of a 5-foot cone at altitudes of 200,000, 150,000 and 100,000 feet, respectively, assuming the boundary layer on the cone surface remains laminar.

CONTENTS

ILLUSTRATIONS

ILLUSTRATIONS (Concl'd)

NOMENCLATURE

Symbols

$F_1, F_2, \ldots$	integrals defined by equations (6) and (7)
h	static enthalpy
H	stagnation enthalpy
j	an index, either 0 or 1
l	$\rho\mu/\rho_1\mu_1$
M	Mach number
N	number of strips
P	pressure
Pr	Prandtl number
r, y	normal coordinate, measured from axis or plane of symmetry
R	gas constant
Re_x	Reynolds number, based on local inviscid properties and x distance.
R_b, d	base radius of body or diameter, respectively
S	Sutherland constant
T	static temperature
u	x-component of velocity
v	r-component of velocity
V	velocity vector
x	streamwise coordinate, measured from forward stagnation point
ρ	mass density

NOMENCLATURE (Concl'd)

Symbols

μ	viscosity
ξ	transformed streamwise coordinate
η	transformed normal coordinate
δ	wake thickness (from axis or plane of symmetry)
θ	momentum thickness, or cone angle
λ	transformed thickness parameter
γ	ratio of specific heats
f	transformed shear function
σ	transformed heat diffusion function

Subscripts

1	evaluated at $f = \delta$ or $\eta = 1$
c	evaluated at $f = 0$ or $\eta = 0$
k	evaluated at edge of kth strip
x, f, η	partial derivative with respect to variable indicated
o	reservoir conditions

I. INTRODUCTION

The flow in the wake of hypersonic vehicles has been the subject of considerable research in recent years. The interest in this subject stems mainly from the realization that the trails of hypersonic vehicles are a potentially significant source of observables, i.e., electrons and radiating species. The bulk of the lieterature deals mainly with the trails of blunt bodies [1, 2, 3] where the viscous core comprises a significant portion of the wake flowfield (from the point of view of observables) only if turbulent mixing is present. However, in the case of slender bodies, the observables in the inviscid flowfield are minimized and the viscous region (laminar or turbulent) becomes the sole source of electrons and radiating species.

An excellent account of the state of the art of the turbulent far wake has been presented by Lees[4] and Vaglio-Laurin, Bloom, and Byrne.[5] These authors extended their blunt-body analyses to the slender-body case. Most analyses of the laminar far wake (shown schematically in figure 1) have been restricted to similar solutions involving linearized forms or to solutions obtained by the Karman-Pohlhausen method. The notable exception is the classical Goldstein solution for the incompressible wake of a flat plate.[6]

Recent experimental data acquired at Avco RAD and the Naval Ordinance Laboratory (NOL) ballistic ranges show appreciable lengths of laminar wake at Reynolds numbers higher than those previously reported.[4] Therefore, for slender bodies a critical analysis of the laminar far wake has a twofold value: (1) to provide detailed flowfields for the prediction of observables, and (2) to compute accurately the appropriate transition parameters.

This paper presents a theoretical analysis of the laminar far wake and also contains some of the experimental results obtained in the Avco RAD ballistic range. The method of theoretical analysis is an extension of the multistrip solution of the laminar boundary-layer equations.[7] No assumptions about the form of the solution are required; only the initial and boundary conditions must be specified. Since no solution of the near wake is presently available, the initial profiles are somewhat arbitrary. However, initial velocity and enthalpy profiles can be prescribed with some degree of confidence from existing knowledge of gross near-wake properties and by utilizing overall momentum and energy conservation. Only pure air wakes in chemical and thermodynamic equilibrium, or completely frozen, are considered in the present analysis. Some results for nonequilibrium wakes have been obtained by Bloom, et al., by the Karman-Pohlhausen technique.[3, 5, 8] The nonsimilar analysis with chemical nonequilibrium has been formulated and some preliminary results obtained[9, 10], but they are not included here.

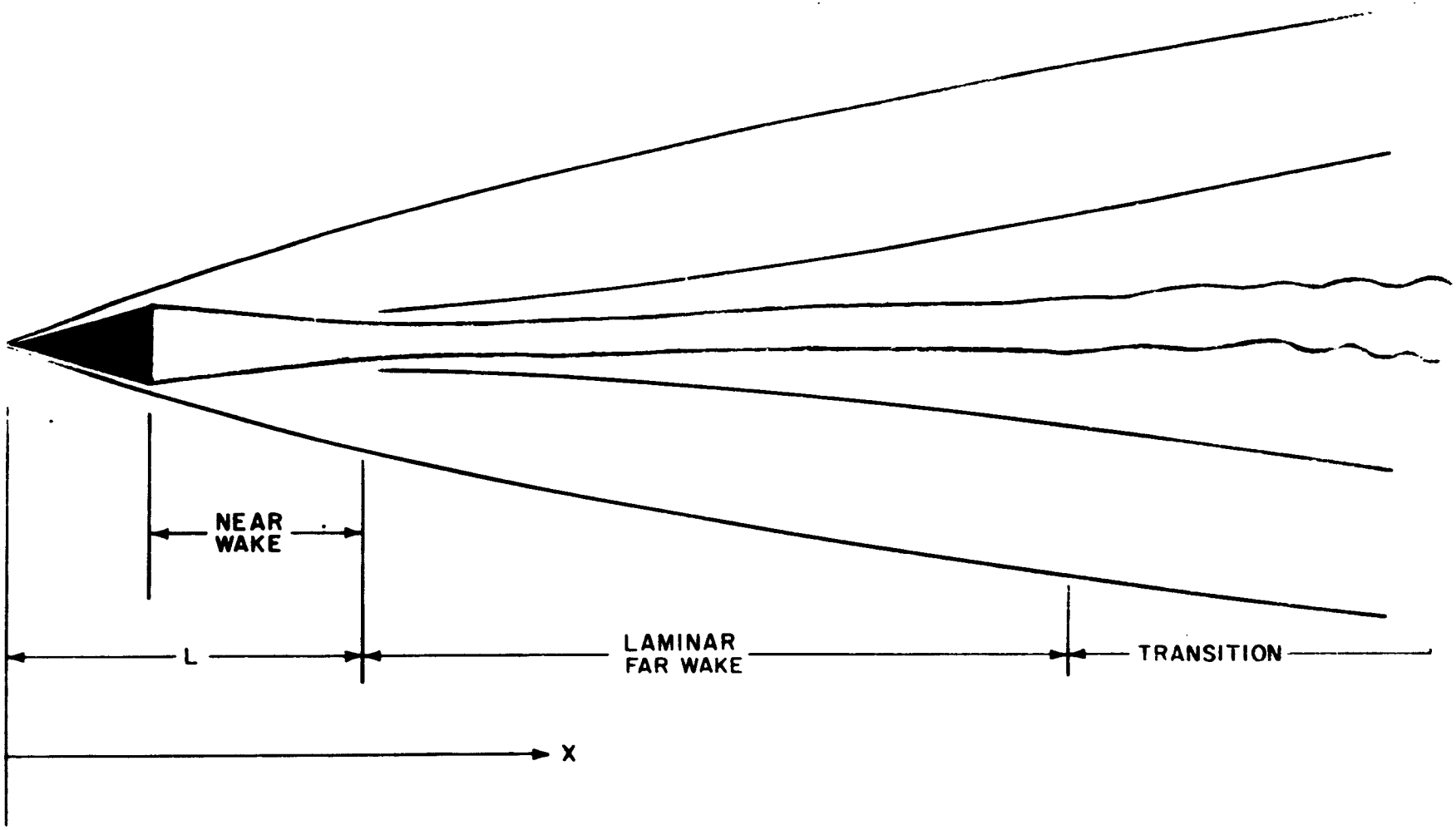

Figure 1 HYPERSONIC SLENDER BODY FLOW FIELD
62-10329

II. NONSIMILAR ANALYSIS

Steady flow downstream of the neck of a wake (i.e., the stagnation point in the wake beyond which no recirculation takes place) can be described in the context of boundary-layer theory by:

$$(\rho u r^j)_x + (\rho v r^j)_r = 0 \tag{1}$$

$$\rho u u_x + \rho v u_r = - p_x + \frac{1}{r^j} (\mu r^j u_r)_r \tag{2a}$$

$$0 = p_y \tag{2b}$$

$$\rho u H_x + \rho v H_r = \frac{1}{r^j} \left\{ \frac{\mu r^j}{Pr} \left[H_r + (Pr - 1) \left(\frac{u^2}{2} \right)_r \right] \right\}_r \tag{3}$$

where

$$j = \begin{cases} 0 \text{ for planar flow} \\ 1 \text{ for axisymmetric flow.} \end{cases}$$

The conventional boundary conditions apply at the outer edge of the wake,

$$\left.\begin{aligned} u = u_1 \text{ and } \frac{\partial u}{\partial r} = 0 \\ H = H_1 \text{ and } \frac{\partial H}{\partial r} = 0 \end{aligned}\right\} \text{ at } r = \delta ,$$

while at the plane or axis of symmetry the boundary conditions are

$$\left.\begin{aligned} u = u_c \text{ and } \frac{\partial u}{\partial r} = 0 \\ H = H_c \text{ and } \frac{\partial H}{\partial r} = 0 \end{aligned}\right\} \text{ at } r = 0$$

Parenthetically, it may be noted at this point that if $P_x = 0$ and $Pr = 1$, the energy equation is satisfied by the Crocco integral:

$$H = Au + B$$

where A and B are constants:

$$A = \frac{H_1 - H_c}{u_1 - u_c}$$

$$B = H_c - \left(\frac{H_1 - H_c}{u_1 - u_c}\right) u_c$$

Therefore:

$$\frac{H_{c_x}}{H_1 - H_c} = \frac{u_{c_x}}{u_1 - u_c}$$

is a particular solution of the energy equation. This solution is, of course, only valid if the initial conditions also satisfy the Crocco integral. The present analysis is not restricted to this case, since the Crocco integral is not employed.

In the present analysis, the wake is divided into an arbitrary number of strips, N, in the streamwise direction, and the equations then are integrated with respect to r across the strips, i.e., between the limits of $r = 0$ and $r = r_k$, to give two ordinary differential equations:*

$$\frac{d}{dx}\left[\rho_1 u_1^2 \int_0^{r_k} \frac{\rho u}{\rho_1 u_1}\left(\frac{u_k}{u_1} - \frac{u}{u_1}\right) r^j\, dr\right] - \rho_1 u_1^2 \left(\int_0^{r_k} \frac{\rho u}{\rho_1 u_1} r^j dr\right) \frac{d}{dx}\left(\frac{u_k}{u_1}\right)$$

$$- \rho_1 u_1 u_k \left(\int_0^{r_k} \frac{\rho u}{\rho_1 u_1} r^j dr\right) \frac{d}{dx}(\ln u_1)$$

$$= \left(\int_0^{r_k} r^j dr\right) \frac{dp}{dx} - \left[u_1 \mu r^j \left(\frac{u}{u_1}\right)_r\right]_0^{r_k} \qquad (4)$$

*The strip-integral method is discussed in greater detail in reference 7.

$$\frac{d}{dx}\left[\rho_1 u_1 \int_0^{r_k} \frac{\rho u}{\rho_1 u_1}\left(\frac{H_k}{H_1} - \frac{H}{H_1}\right) r^j \, dr\right] - \rho_1 u_1 \left(\int_0^{r_k} \frac{\rho u}{\rho_1 u_1} r^j \, dr\right) \frac{d}{dx}\left(\frac{H_k}{H_1}\right)$$

$$= -\left\{\frac{\mu r^j}{Pr}\left[\left(\frac{H}{H_1}\right)_r + (Pr - 1)\frac{u_1^2}{2H_1}\left(\frac{u}{u_1}\right)_r^2\right]\right\}_0^{r_k} \qquad (5)$$

The transformed independent variables $\xi, \eta,$ are now introduced

$$\xi = \frac{x}{L}$$

$$\eta = \left(\frac{j+1}{\delta_t^{j+1}} \int_0^r \frac{\rho}{\rho_1} r^j \, dr\right)^{\frac{1}{j+1}}$$

where L is a characteristic length of the problem and

$$\delta_t = \left((j+1) \int_0^{\delta} \frac{\rho}{\rho_1} r^j \, dr\right)^{\frac{1}{j+1}}$$

is the thickness of the velocity and thermal profiles in the transformed plane.

The equations now become

$$\left(\frac{j+1}{2}\right) F_{1_k} \frac{d\lambda}{d\xi} + \lambda \frac{dF_{1_k}}{d\xi} - \lambda F_{2_k} \frac{d}{d\xi}\left(\frac{u_k}{u_1}\right) + \left[\left(\frac{j+1}{\eta_k}\right)\left(\frac{\mu_1}{\rho_1 u_1 L}\right)^{1/2} F_{3_k}\right]^{j} (l_k \eta_k - l_c r_c)$$

$$= -\lambda \left[F_{1_k} \frac{d}{d\xi} \ln (\rho_1 u_1 \mu_1)^{1/2} + \left(F_{1_k} - \frac{u_k}{u_1} F_{2_k} + F_{3_k}\right) \frac{d}{d\xi} \ln u_1\right] \tag{6}$$

$$\left(\frac{j+1}{2}\right) F_{4_k} \frac{d\lambda}{d\xi} + \lambda \frac{dF_{4_k}}{d\xi} - \lambda F_{2_k} \frac{d}{d\xi}\left(\frac{H_k}{H_1}\right) + \left[\left(\frac{j+1}{\eta_k}\right)\left(\frac{\mu_1}{\rho_1 u_1 L}\right)^{1/2} F_{3_k}\right]^{j} \frac{l_k}{Pr}\left[\sigma_k + \frac{u_1^2}{H_1}(Pr-1)\frac{u_k}{u_1} r_k\right]$$

$$- \frac{l_c}{Pr}\left[\sigma_c + \frac{u_1^2}{H_1}(Pr-1)\frac{u_c}{u_1} r_c\right] = -\lambda F_{4_k} \frac{d}{d\xi} \ln (\rho_1 u_1 \mu_1)^{1/2}, \tag{7}$$

where

$$\lambda = \left(\frac{\rho_1 u_1 L}{\mu_1}\right)^{\frac{1}{j+1}} \left(\frac{\delta_t}{L}\right)^2$$

$$r = \left(\frac{u}{u_1}\right)_\eta$$

$$\sigma = \left(\frac{H}{H_1}\right)_\eta$$

$$l = \frac{\rho \mu}{\rho_1 \mu_1}$$

$$\eta_k \quad \frac{1 + (N - k)}{N} \quad , \; k = 1, 2, 3, \ldots, N$$

$$F_{1_k} = \int_0^{\eta_k} \frac{u}{u_1} \left(\frac{u_k}{u_1} - \frac{u}{u_1} \right) \eta^j \, d\eta$$

$$F_{2_k} = \int_0^{\eta_k} \frac{u}{u_1} \, \eta^j \, d\eta$$

$$F_{3_k} = \int_0^{\eta_k} \frac{\rho_1}{\rho} \, \eta^j \, d\eta$$

$$F_{4_k} = \int_0^{\eta_k} \frac{u}{u_1} \left(\frac{H_k}{H_1} - \frac{H}{H_1} \right) \eta^j \, d\eta$$

The transformed boundary conditions are

$$\left.\begin{aligned} \frac{u}{u_1} &= 1 \text{ and } \left(\frac{u}{u_1}\right)_\eta = 0 \\ \frac{H}{H_1} &= 1 \text{ and } \left(\frac{H}{H_1}\right)_\eta = 0 \end{aligned}\right\} \text{ at } \eta = 1$$

$$\left.\begin{aligned} \frac{u}{u_1} &= \frac{u_c}{u_1} \text{ and } \left(\frac{u}{u_1}\right)_\eta = 0 \\ \frac{H}{H_1} &= \frac{H_c}{H_1} \text{ and } \left(\frac{H}{H_1}\right)_\eta = 0 \end{aligned}\right\} \text{ at } \eta = 0 \; .$$

Moreover, the transformed momentum and energy equations evaluated at $\eta = 0$ become*

$$\frac{u_c}{u_1}\frac{d}{d\xi}\frac{u_c}{u_1} - \frac{(j+1)\,l_c\left[\left(\frac{u}{u_1}\right)_{\eta\eta}\right]_c}{\lambda\left(\frac{\rho_c}{\rho_1}\right)^j\left(\frac{\rho_1 u_1 L}{\mu_1}\right)^{j/2}} = \left[\frac{\rho_1}{\rho_c} - \left(\frac{u_c}{u_1}\right)^2\right]\frac{d}{d\xi}\ln u_1$$

and

$$\frac{u_c}{u_1}\frac{d}{d\xi}\left(\frac{H_c}{H_1}\right) - \frac{(j+1)\,l_c}{\lambda\left(\frac{\rho_c}{\rho_1}\right)^j\left(\frac{\rho_1 u_1 L}{\mu_1}\right)^{1/2}}\left\{\left[\left(\frac{H}{H_1}\right)_{\eta\eta}\right]_c + (Pr-1)\,\frac{u_1^2}{H_1}\left(\frac{u_c}{u_1}\right)\left[\left(\frac{u}{u_1}\right)_{\eta\eta}\right]_c\right\} = 0$$

The velocity and stagnation enthalpy profiles can be expressed as polynominals in η. However, additional numerical accuracy can be obtained by choosing the following:

$$\frac{u}{u_1} = 1 + e^{\frac{-\eta}{1-\eta}}\sum_{n=0}^{N} a_n \eta^n$$

$$\frac{H}{H_1} = 1 + e^{\frac{-\eta}{1-\eta}}\sum_{n=0}^{N+1} b_n \eta^n$$

which identically satisfy the imposed boundary conditions at $\eta = 1$ (and moreover satisfy the requirement that all higher-order derivatives also vanish at that

---

*Note that $\lim_{r\to 0}\frac{\mu u_r}{r} = (\mu u_{rr})_{r=0}$.

point). The polynominal coefficients are made to satisfy the boundary conditions at $\eta = 0$ and the values of u_k and H_k at the strip boundaries and at the wake axis, or plane of symmetry, and also $H_{\eta\eta_c}$.

The ordinary equation of state, $P = \rho RT$, provides the necessary thermodynamic relations for a perfect gas, while curvefits of the Mollier chart[14] can be employed for equilibrium air.

Frozen flow can be approximated by the use of the perfect gas law with appropriate gas constant, R, and ratio of specific heats, γ. At low temperatures, the Sutherland viscosity law is employed to give

$$l_k = \left(\frac{T_k}{T_1}\right)^{1/2} \left[\frac{1 + S/T_1}{T_k/T_1 + S/T_1}\right] \text{(including k = c)}$$

where

$$S = 120^\circ K$$

while at elevated temperatures the $\rho\mu$ ratio is approximated by

$$l_k = \frac{A\left(\frac{h_k}{h_r}\right)^{-1/2} - B\left(\frac{h_k}{h_r}\right)^{-1}}{A\left(\frac{h_1}{h_r}\right)^{-1/2} - B\left(\frac{h_1}{h_r}\right)^{-1}} \quad \text{(including k = c)}$$

where

$$A = 3.03$$

$$B = 2.03$$

$$h_r = 4.5 \times 10^6 \text{ ft}^2/\text{sec}^2.$$

Therefore, 2N + 2 first-order ordinary differential equations are obtained (N momentum integral, N energy integral, and momentum and energy at $\tau = 0$)

which can be solved numerically for the $2N + 2$ unknowns (λ, u_k, H_k, for $k = 2, 3, \ldots, N$, and u_c, H_c and $H_{\eta\eta c}$). A predictor-corrector marching scheme is employed for solution of the equations on an IBM 7094.*

*It is important to note that in a numerical solution equations (8) and (9) are singular for $u_c = 0$, although as pointed out by T. Kubota (in private communication), this difficulty can be avoided in an analytical solution by use of an appropriate, nonzero pressure gradient. The behavior of the equations near this rear stagnation point has been examined by S.I. Cheng (Avco RAD-TM-63-23) and by Vaglio-Laurin, Bloom and Byrne[5]. In the present analysis, solution of the equations is always begun slightly away from the stagnation point, with a small but finite value of u_c.

III. COMPARISON OF METHODS OF APPROACH TO THE FLUID DYNAMICS OF THE WAKE

The laminar wake of a slender body only recently has gained practical importance as a fluid-dynamic problem due to its apparent high stability at hypersonic speeds* which has not been previously observed. However, computations of the laminar wake of a thin flat plate at low speeds were reported in the 1930's (e. g., reference 6), and various approximate methods have been developed. The only "exact" solution, however, is that of Goldstein,[6] which is essentially a finite difference solution for the wake in the immediate vicinity of the trailing edge. The approximate methods which have been developed fall into essentially two categories--(1) the "similarity" solutions, and (2) the Karman-Pohlhausen-type solutions.

The similarity analyses require linearization of the velocity defect $(u_1 - u)$ and usually neglect the streamwise pressure gradients, which results in a closed-form solution of the partial differential equations of momentum and energy satisfying the wake-boundary conditions. The effect of initial conditions is felt only through two constants in the solution, which are usually defined by overall momentum and energy conservation from the body boundary layer.

The Karman-Pohlhausen-type analysis, as the name implies, is an extension of the integral boundary-layer approach to the wake problem. Clearly, the accuracy of an integral-type solution is dependent on its ability to represent the detailed behavior of properties across the layer, which is a function of the number of independent, free parameters retained in the solution. ** In the Karman-Pohlhausen method, the only free (undetermined) parameters are usually the thickness δ, the velocity, and enthalpy on the axis, or plane, of symmetry, u_c and H_c, and the curvature of the enthalpy profile at the axis $H_{\eta\eta_c}$. Hence, the only nonsimilar influence on the normalized velocity profile $\left(\frac{u-u_c}{u_1-u_c}\right)$ is the thickness δ, and the only influence on the normalized enthalpy profile $\left(\frac{H-H_c}{H_1-H_c}\right)$ is due to δ and the curvature of the profile at the axis. The initial conditions are specified through the initial values of the free parameters. The momentum-integral equation itself is no more than an expression of the fact that the drag contained in the wake is constant, implying that in a numerical integration of the equations the initial conditions must reflect the correct drag (i. e., initial momentum thickness) to guarantee the proper integration constant. In the Karman-Pohlhausen technique, this requirement can cuase a mismatch of the overall thickness, depending on the shape of the initial profile being approximated.

*Discussed in further detail later.

**Reference 8 is an excellent example of the use of the Karman-Pohlhausen technique in studying nonequilibrium viscous flow problems.

The present method also is categorized as an integral method (being, in fact, an application of Dorodnitsyn's "method of integral relations") and, as such, is an approximate method also. However, it avoids the restrictions associated with the Karman-Pohlhausen method since the velocity and enthalpy on the strip boundaries are additional free parameters which must be determined from the differential equations.

The problem of the laminar wake of a thin flat plate was examined in detail to compare the approximate methods mentioned above and the present method with the classical Goldstein solution. This problem also has the feature that there is no recirculation and the initial (Blasius) profile is known exactly. The decay of the velocity along the plane of symmetry and typical velocity profiles are illustrated in figures 2 and 3.* The similarity solutions give $\left(1 - \frac{u_c}{u_1}\right) \sim 1/x^{1/2}$ which is particularly poor near the trailing edge, although the rate is correct asymptotically at large distances. The Karman-Pohlhausen method shows remarkably good agreement with the exact results near the center of the wake in this case. Some differences in thickness δ are illustrated in figure 4. The present method, however, is in essentially perfect agreement with Goldstein's solution. It should be noted that the results from the present method shown were obtained with six strips, but calculations also were performed with two through five strips. Rapid convergence of the solution was obtained with greater than four strips, although two strips offered little improvement over the Karman-Pohlhausen (one strip) solution.

*The reference length L is taken as the plate length in this case.

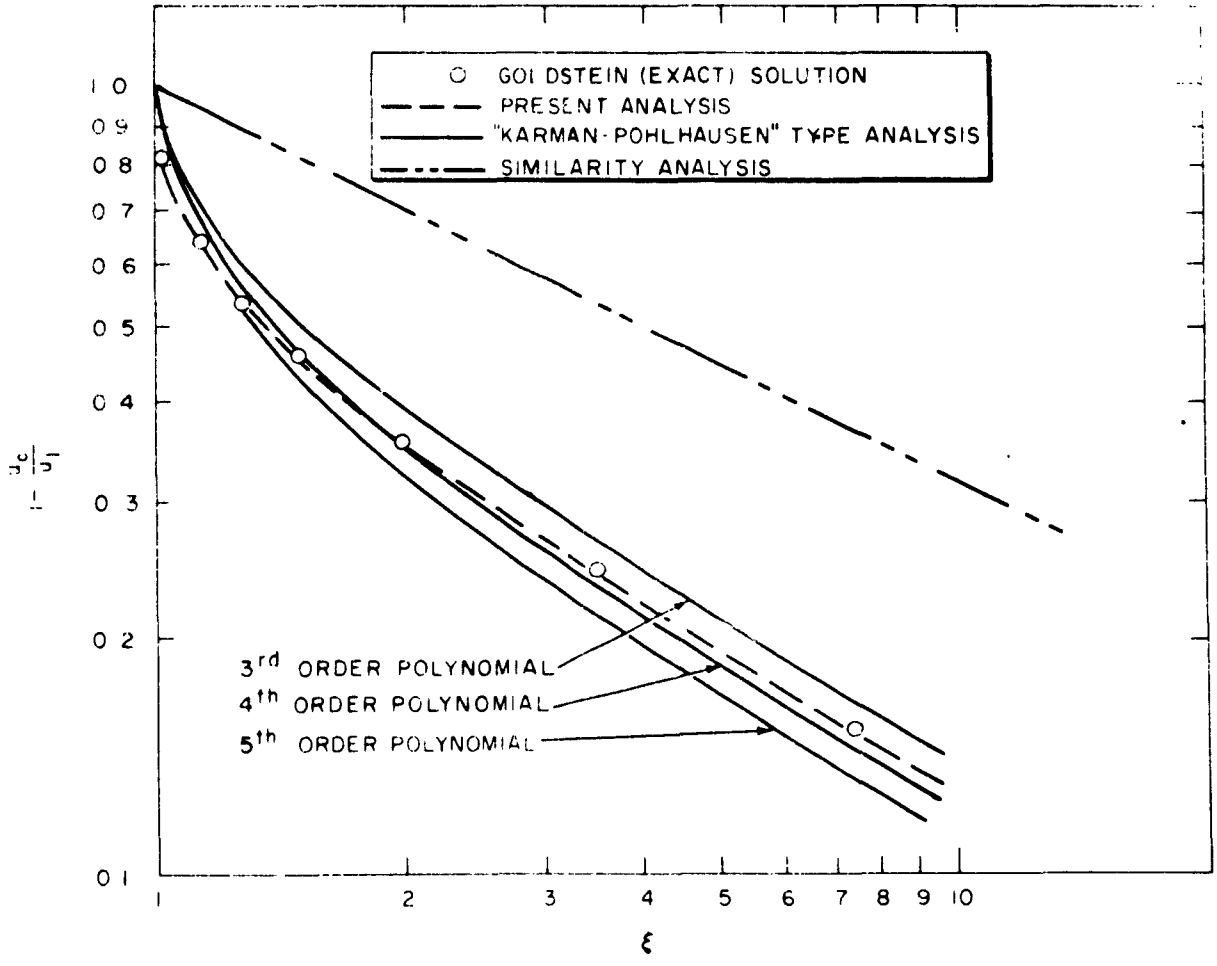

Figure 2 INCOMPRESSIBLE LAMINAR WAKE OF A FLAT PLATE
63-4981

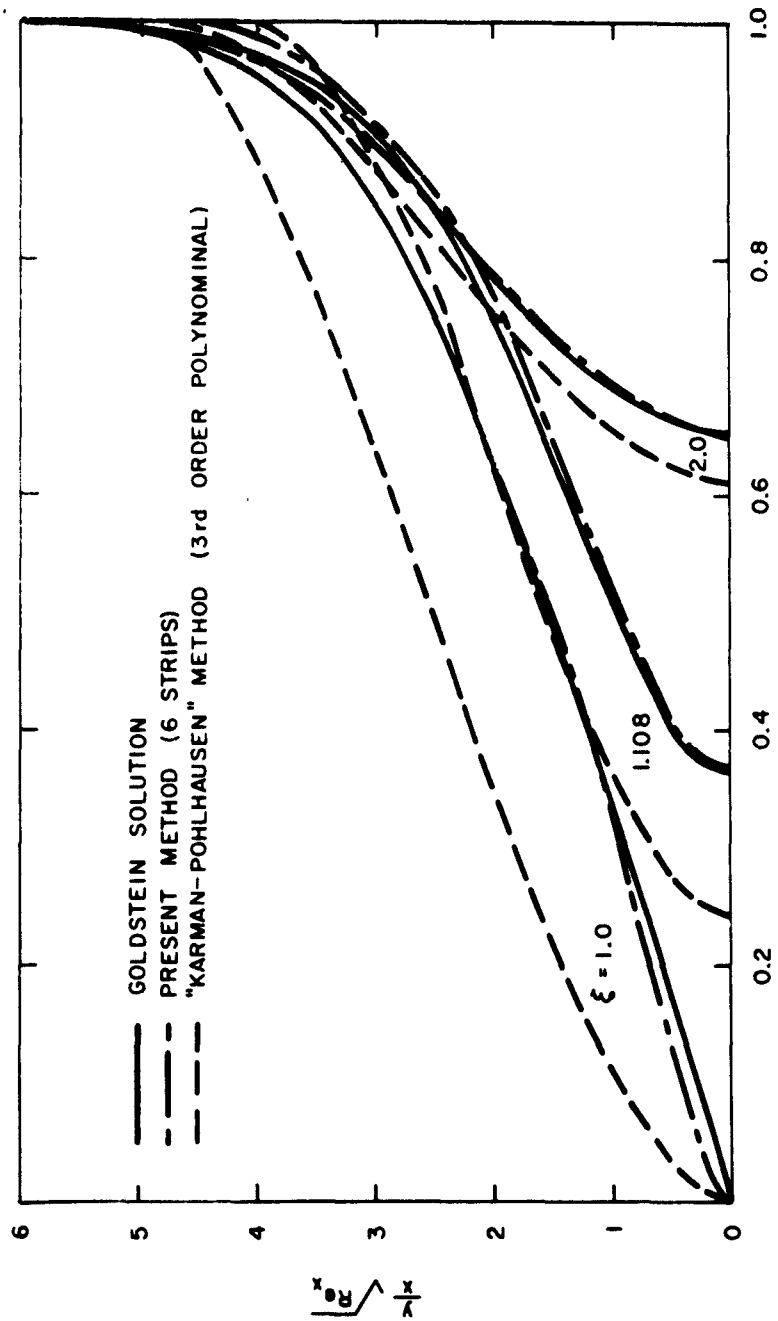

Figure 3 VELOCITY PROFILES IN THE WAKE OF A FLAT PLATE
63-3488

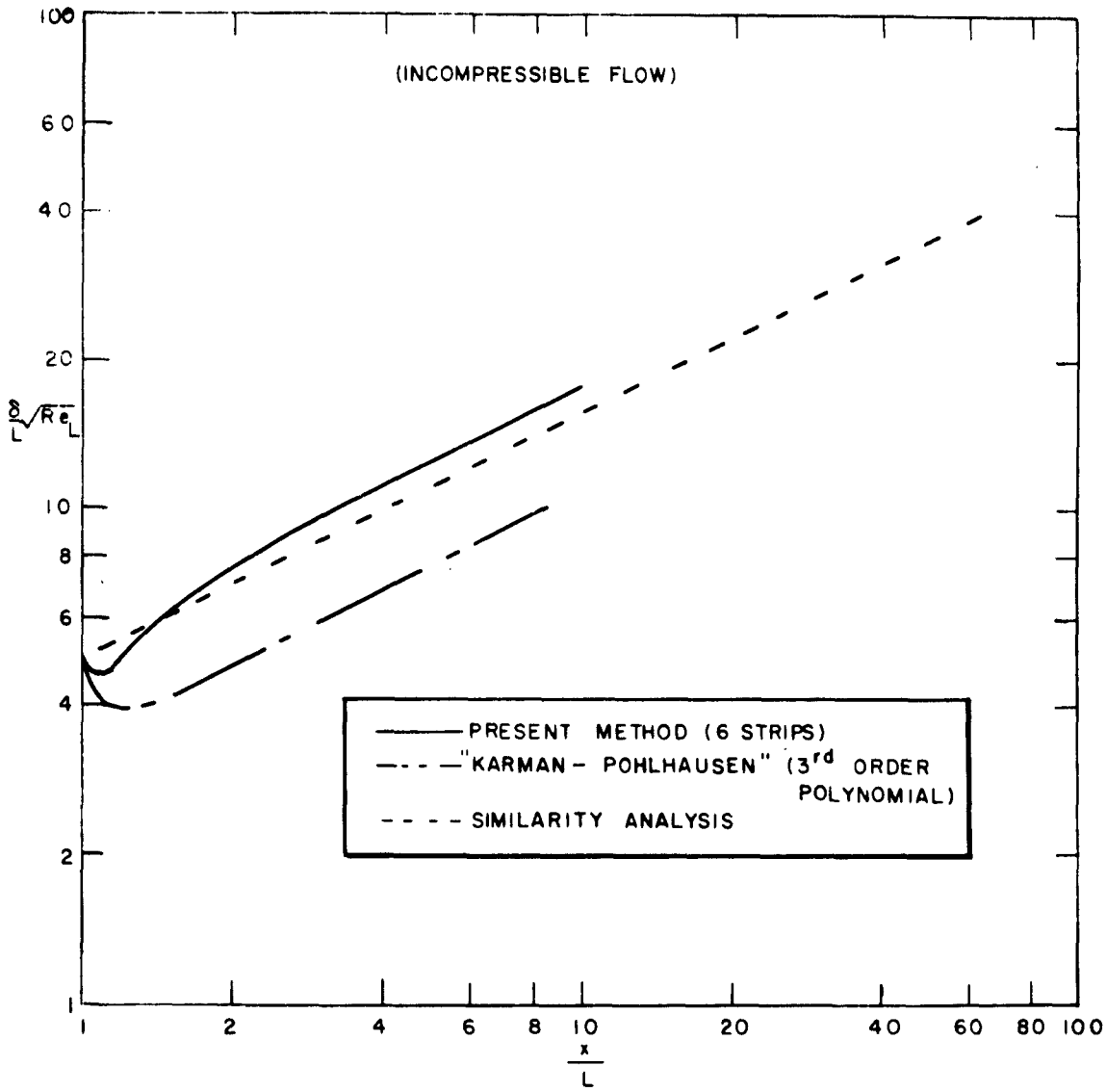

Figure 4 GROWTH OF THE WAKE OF A FLAT PLATE
63-4980

IV. HYPERSONIC LAMINAR FAR WAKE FOR A SLENDER BODY

A. INITIAL (NECK) CONDITIONS

The conditions which occur at the neck of the hypersonic wake are the result of simultaneous mixing and recirculation of the boundary layer shed from the body, as well as a strong adverse pressure gradient (which "drives" the recirculating flow). Also, the base of the body is a stagnation point which has been experimentally observed to have many of the features (e.g., high heat flux) of a blunt-body stagnation point, although less severe. Unfortunately, the near wake has thus far eluded successful theoretical treatment, but it is currently receiving considerable attention. Various approximations have been attempted, but none offer any really satisfactory insight into the mechanism or magnitude of the recirculation and base heating.

The mixing phenomenon per se has been treated by Denison and Baum, [11] Vaglio-Laurin, Bloom and Byrne [5] as an extension of the earlier ideas of Chapman, [12] who studied the mixing of a stream with quiescent air. Chapman's analysis assumed a zero-thickness shear layer at the beginning of the mixing region, for which he obtained a value of $\frac{u^*}{u_1} = 0.587$ for the velocity ratio of the dividing streamline.* Denison and Baum considered the supersonic mixing process starting with a Blasius profile and both cold quiescent air (free-stream static temperature) and hot quiescent air (free-stream stagnation temperature) for a variety of cone and wedge angles. Their results indicate that the dividing streamline velocity ratio is on the order of 0.25 to 0.20 at hypersonic speeds for 10-to 20-degree cones for the cold case, and 0.35 to 0.30 for the hot case. With constant-temperature quiescent air,**constant pressure mixing, and Prandtl number of unity, the Crocco integral is a solution of the energy equation, giving:

$$\frac{H^*}{H_1} = \left(1 - \frac{H_b}{H_1}\right)\left(\frac{u^*}{u_1}\right) + \frac{H_b}{H_1}$$

where

H^* = dividing streamline total enthalpy

H_b = total enthalpy of the quiescent air

H_1 = total enthalpy of the inviscid stream.

*The streamline which separates the flow which passes the neck from the recirculating flow.

**At approximately the body wall temperature.

For the cold case, $\frac{H_b}{H_1} \ll 1$, giving $\frac{H^*}{H_1} \approx \frac{u^*}{u_1}$. Clearly, in the hot case $\frac{H^*}{H_1} \approx 1$. Therefore, consideration of the mixing process alone leads to a realistic lower limit on the dividing streamline enthalpy. Assuming that the compression process occurs through a shocklike discontinuity (allowing the neglect of viscous dissipation), then the dividing streamline enthalpy can be taken as the value occurring on the axis at the neck (i.e., where the dividing streamline is stagnated).

The nature of the compression process in the neck region suggests that the neck bears certain similarities to a boundary-layer separation point. (Indeed, it has been recognized by various authors that gross properties such as base pressure and wake angle are predictable in terms of separation-point pressure correlations.) Therefore, the use of a separation-point velocity profile from similarity solutions such as Cohen and Reshotko[13] appears to be a reasonable approximation. However, the enthalpy profile which would result after such a compression is not known beyond the axis value indicated above. Clearly, the use of the Crocco integral is not correct for the entire near wake, a region which includes strong pressure gradients; but, it does have the justification of being at least a consistent means of approximating the neck enthalpy profile in terms of the assumed velocity profile and the (approximately) known enthalpy on the axis. However, it should be noted that the use of the Crocco integral leads to an "annulus" of high temperature gas rather than a "cylinder" at the neck for slender bodies. It is not obvious whether this is physically reasonable; intuitively, it would be expected that the peak temperature would occur at the axis. Regardless, for the lack of any better knowledge of the near wake, the Crocco integral will be used in the present analysis to specify the initial total enthalpy.

The necessity of matching the initial drag (i.e., momentum thickness) at the neck has been previously mentioned. Assuming, a priori, that the drag added in the near wake is negligible in comparison with that shed from the body in the boundary layer, the initial momentum thickness is given by:

$$[\rho_1 u_1^2 \theta^{j+1}]_{neck} = [\rho_1 u_1^2 (j+1) R_b^j \theta]_{body}$$

where

$$\theta_{neck} = \left\{ (j+1) \int_0^{\delta} \frac{\rho u}{\rho_1 u_1} \left(1 - \frac{u}{u_1}\right) r^j \, dr \right\}^{1/j+1}$$

In the numerical examples the initial value of the thickness parameter, λ , is computed from the neck momentum thickness in the following manner:

$$\lambda = \left(\frac{\theta}{L}\right)^2 \left\{ \frac{Re_L^{1/2}}{(j+1)\, F_{1_1}} \right\}^{2/j+1}$$

The above assumptions are verified a posteriori only in that they lead to results which are in good agreement with the experimentally observed facts (i. e., the wake thickness and its Reynolds-number dependence), which is discussed in greater detail later in this paper. However, when they are applied at very low pressures (high altitude) certain anomalous results are obtained, namely initial wake thicknesses which exceed the body diameter and even the "displaced" body diameter (i. e., body plus boundary layer). This is undoubtedly due to neglect of interaction with the individual flow. The viscous-inviscid interaction is a separate problem which is not considered in this analysis, nor in any of the examples.

B. NUMERICAL EXAMPLES

The present analysis was applied to study the development of the laminar far-wake for some typical cases of interest. The medium is assumed to be air in equilibrium, unless otherwise noted, with a constant Prandtl number of 0. 72.

The following case is an example which is typical of experiments performed in the Avco RAD ballistics range:

10-degree (semivertex angle) cone
base diameter: 0. 300 inch
velocity: 15, 688 ft./sec
pressure: 150 mmHg

Velocity and temperature profiles (with $\frac{H_c}{H_1} = 0.3$ initially) for the wake at these conditions are shown in figures 5 and 6. The features of the flowfield which can be observed from the Schlieren photos (e. g., figure 14, the thickness and growth rate) are essentially in agreement with these results.

This slender axisymmetric body example may be contrasted to the results for a blunt semi-infinite body; namely, a cylinder placed normal to the flow. The conditions selected correspond to one of the experiments performed by McCarthy in the GALCIT with tunnel:[16]

0. 300-inch-diameter cylinder
free-stream Mach number: 5. 7
reservoir pressure: 35 psig
reservoir temperature: 262°F

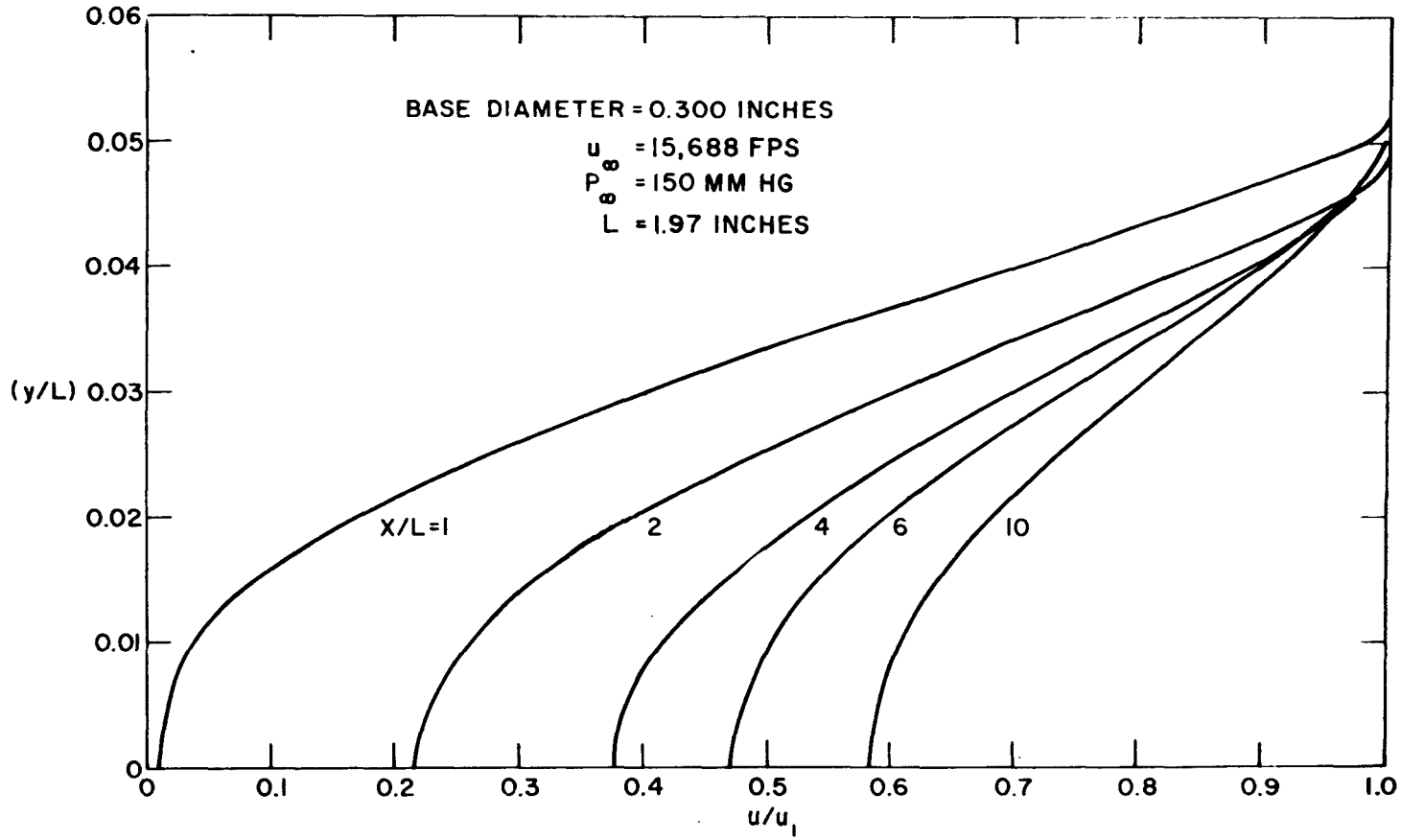

Figure 5 VELOCITY PROFILES IN THE EQUILIBRIUM WAKE OF A 10-DEGREE CONE
63-3501

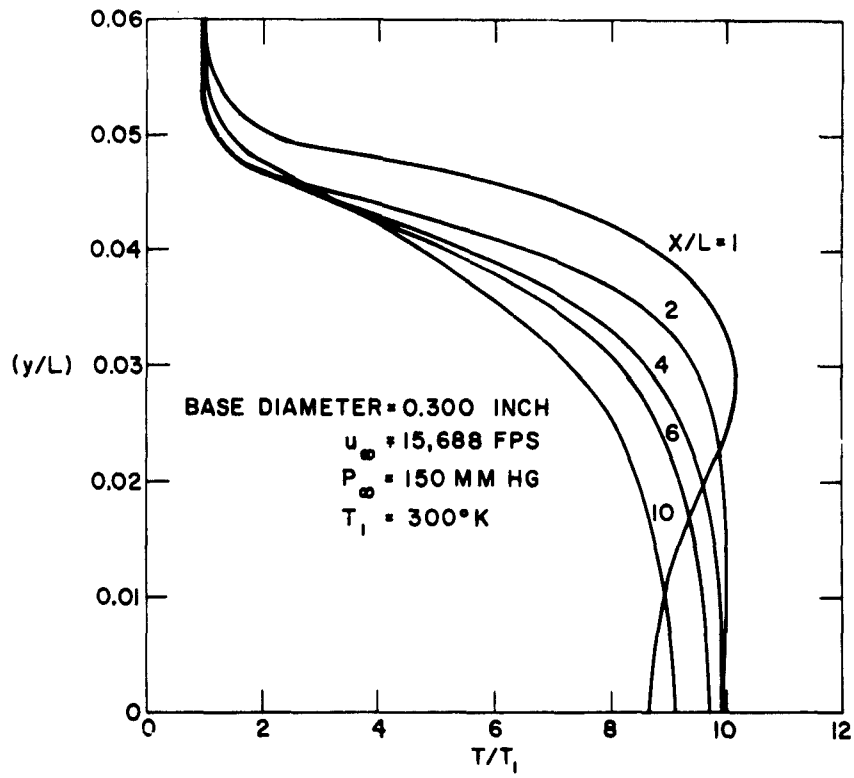

Figure 6 TEMPERATURE PROFILES IN THE EQUILIBRIUM WAKE OF A 10-DEGREE CONE
63-3502

In this case, the viscous core may entrain mass flow from the entropy layer as it grows. This "swallowing" effect was estimated using the method of characteristics. It was found, however, that the laminar core (in the present example) does not entrain any appreciable mass from the entropy layer for at least 25 diameters from the neck. An appreciable velocity gradient is encountered, nonetheless, due to the presence of expansion waves reflected from the bow shock.

A constant stagnation enthalpy (equal to the free-stream value) was assumed, since the tunnel running time was long allowing the model to approach an equilibrium temperature. Typical resulting velocity and temperature profiles are shown in figures 7 and 8. The very fast velocity decay observed here is similar to that found in the classical flat-plate solution, and appears to be peculiar to semiinfinite bodies. The relative importance of the nonsimilar behavior of the solution and also of the attendant favorable pressure gradient in this example are illustrated in figure 9. As much as a 70-percent error can be attributed to neglect of the pressure gradient.* It should also be noted that no effect of Reynolds number on the decay rates can be expected (also, as in the flat-plate case) if the initial value of the thickness parameter λ is constant, as indicated by McCarthy's data.

As an example for the laminar far wake of a slender body at flight conditions, a constant velocity (22,000 ft/sec) trajectory from 200,000 to 100,000 feet was assumed for a 10-foot, 12-degree (semivertex) angle cone. An initial enthalpy ratio of $\frac{H_c}{H_1} = 0.3$ was assumed and the calculations were performed for both frozen ($\gamma = 1.4$ and $R = 1,724$ ft^2/sec^2 / $^\circ$R) and equilibrium air. Typical profiles and the velocity and temperature along the wake axis are given in figures 10, 11, 12, and 13. The results are qualitatively similar to those for the previous slender-body example. It is interesting to note the growth in length of the trail with decreasing altitude. However, at 200,000 feet the initial thickness exceeds the body diameter by about 30 percent. Consideration of the interaction phenomena should lead to a shorter trail at this altitude. (The equilibrium results at 200,000 feet and the frozen results at 100,000 feet are included only for comparison's sake; clearly neither are physically realistic.)

*Attention must be called to the fact that much smaller pressure gradients are encountered with slender, sharp cones.

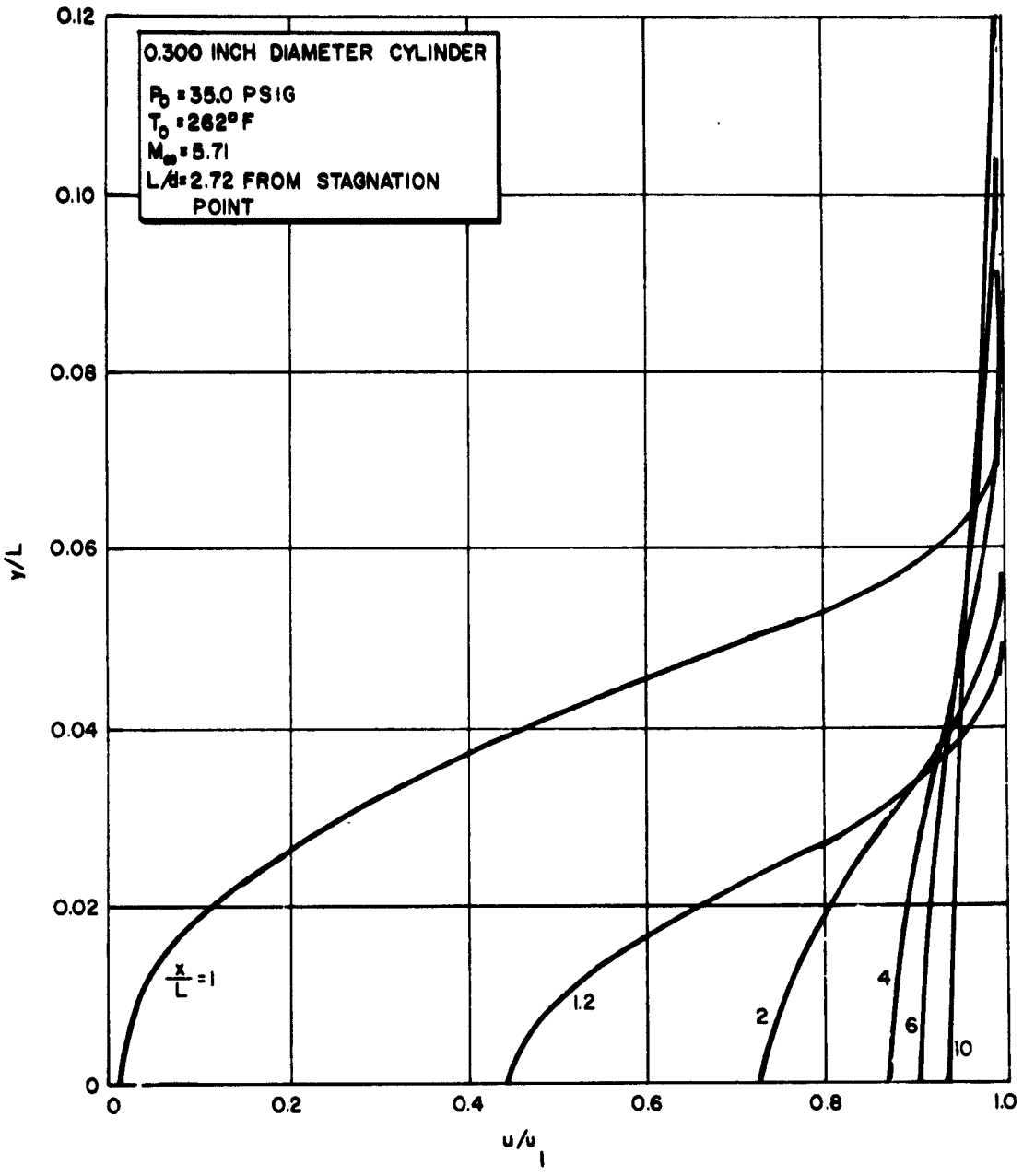

Figure 7 VELOCITY PROFILES IN THE WAKE OF A CYLINDER
63-4983

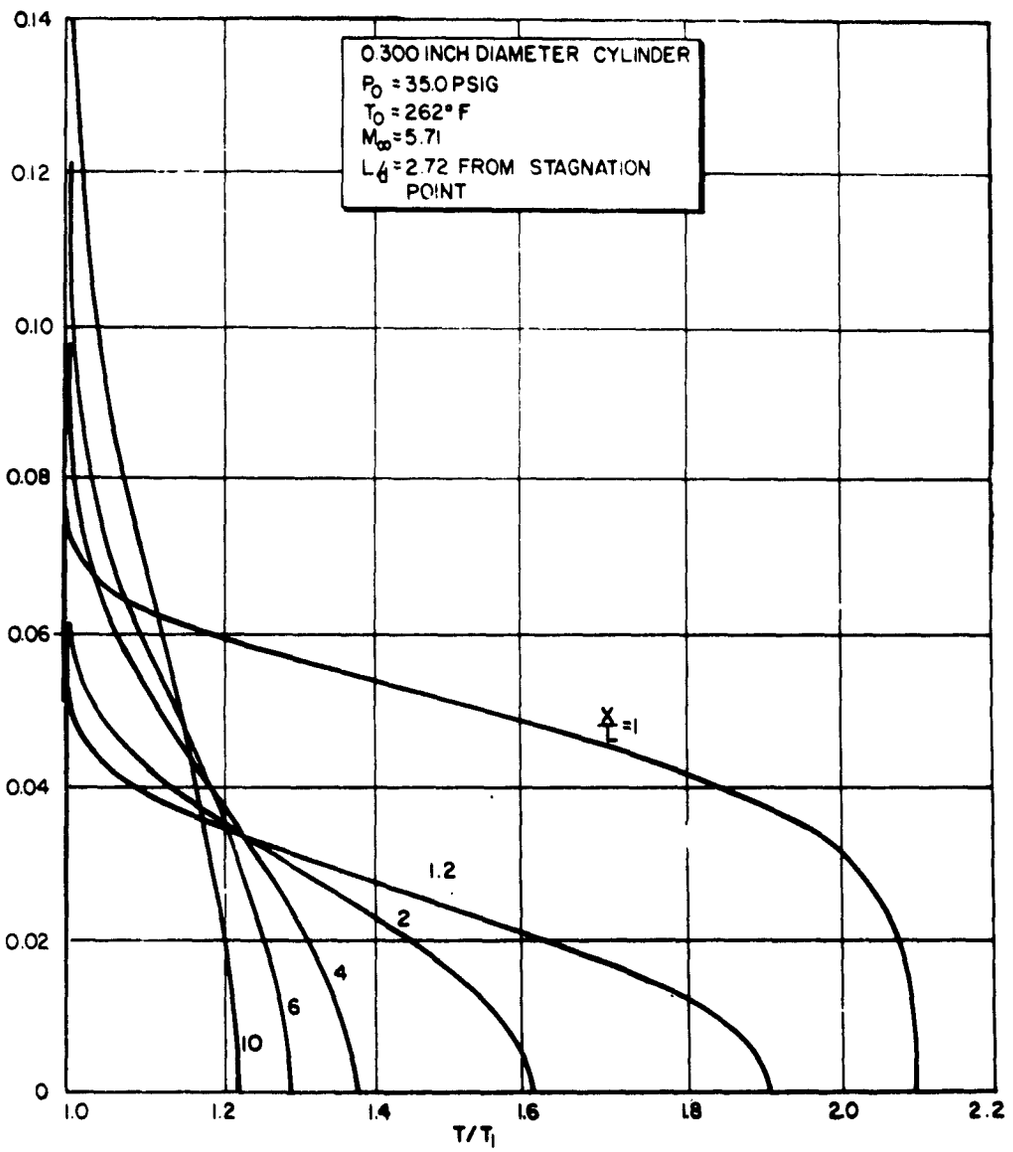

Figure 8 TEMPERATURE PROFILES IN THE WAKE OF A CYLINDER
63-4984

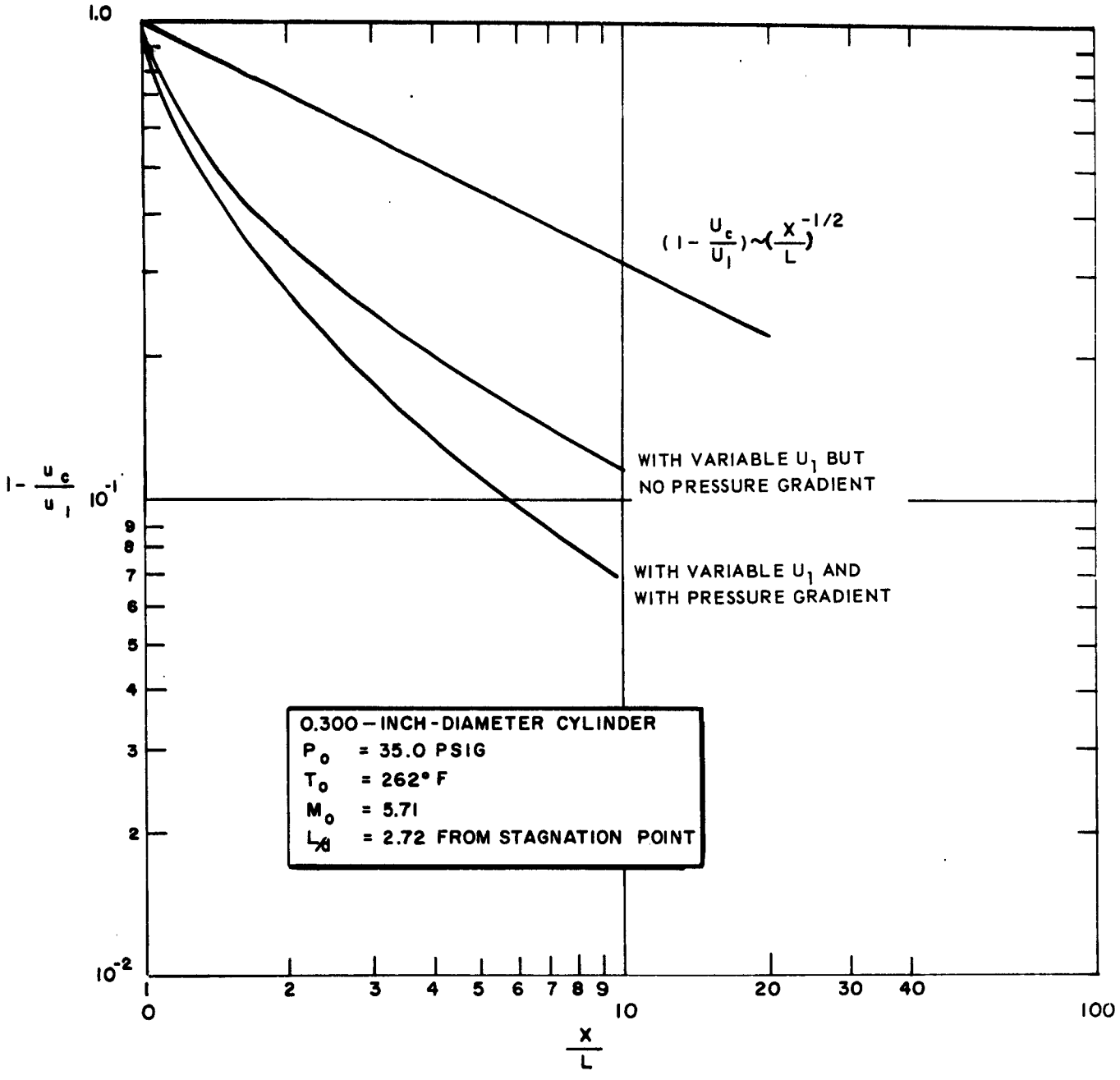

Figure 9 VELOCITY DECAY IN THE WAKE OF A CYLINDER

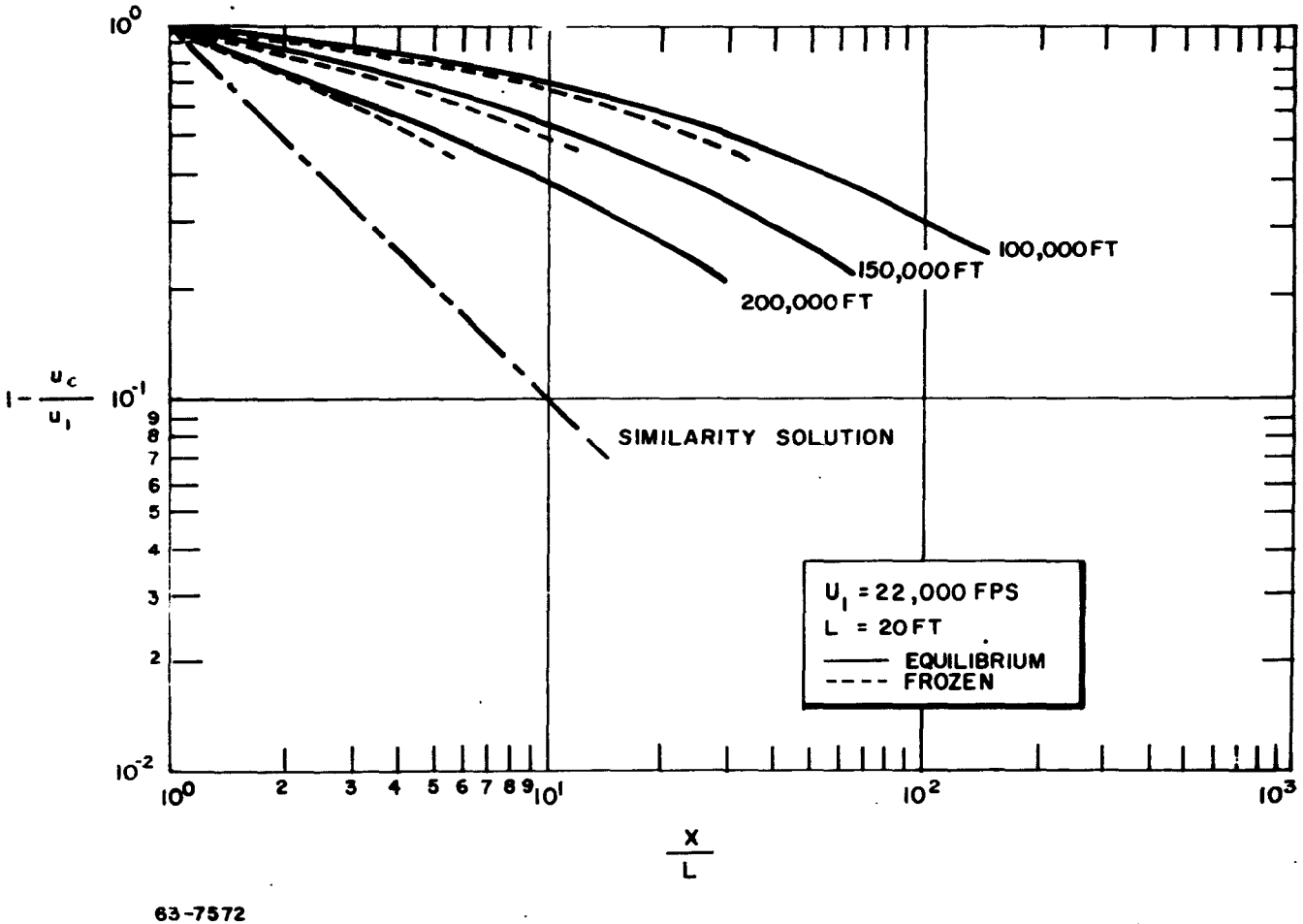

Figure 10 VELOCITY DECAY ALONG THE WAKE AXIS OF A 10-FOOT, 12-DEGREE CONE

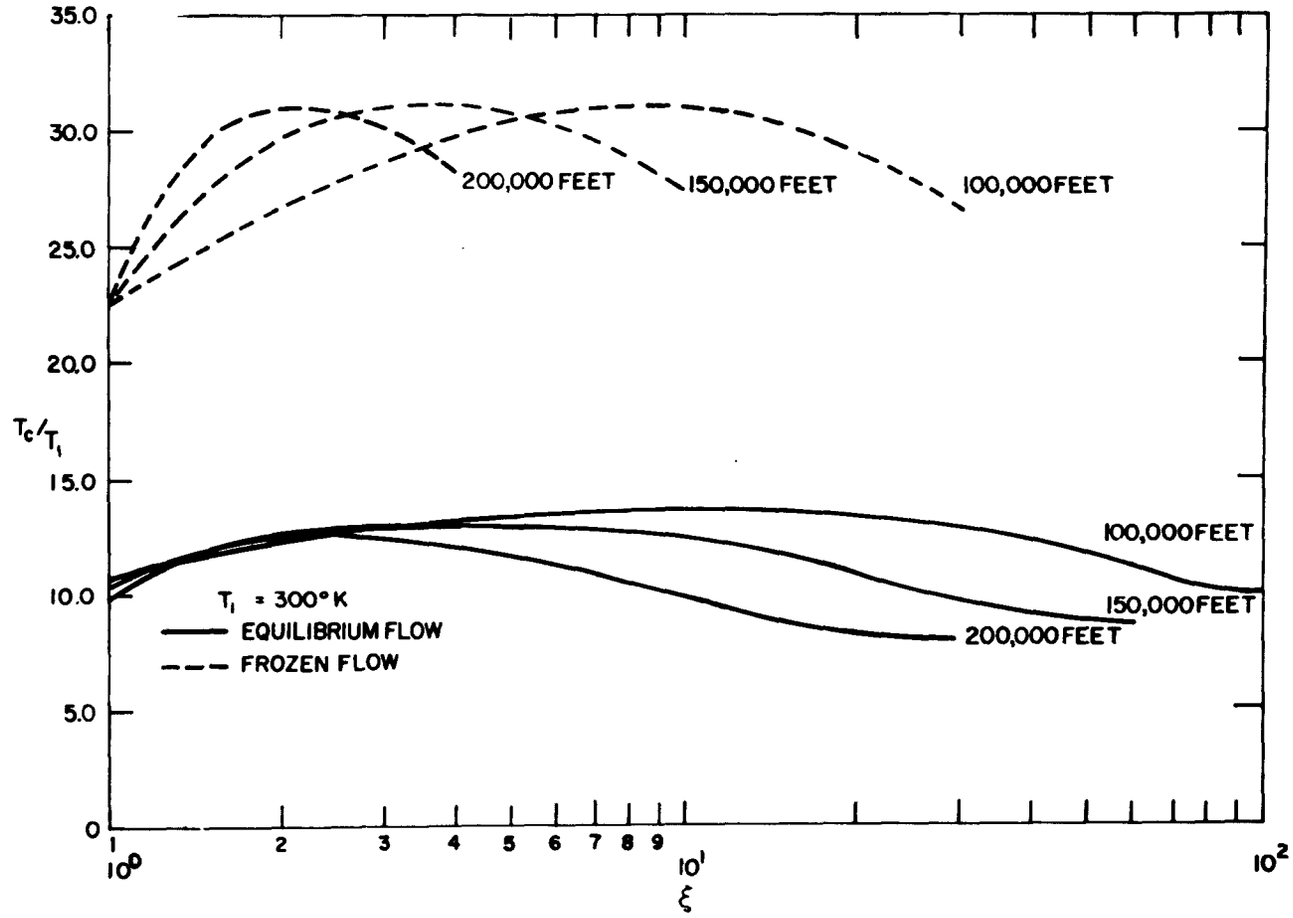

Figure 11 TEMPERATURE DECAY ALONG THE WAKE AXIS OF A 10-FOOT 12-DEGREE CONE
63-4376

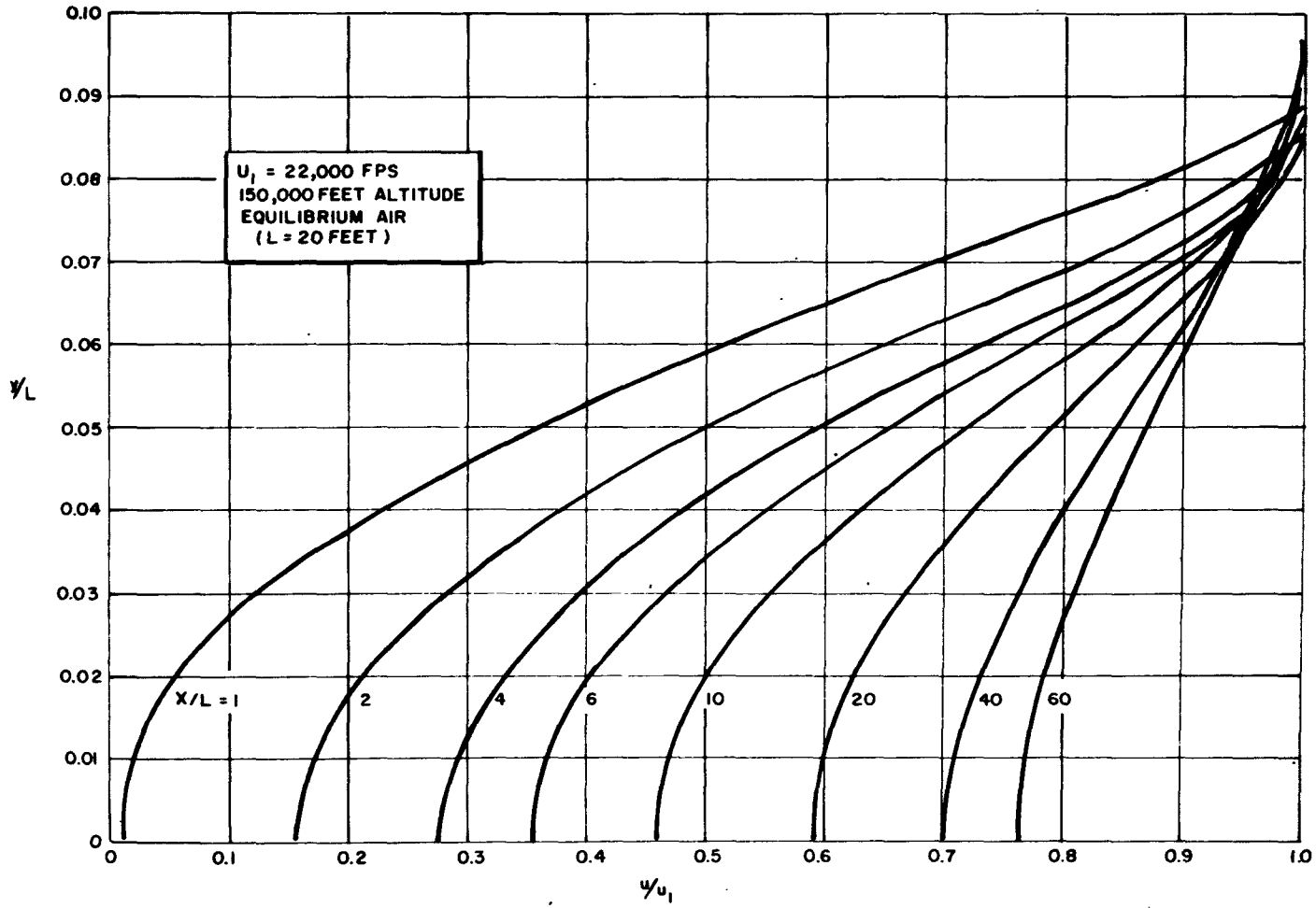

63-7571

Figure 12 VELOCITY PROFILES IN THE WAKE OF A 10-FOOT, 12-DEGREE CONE

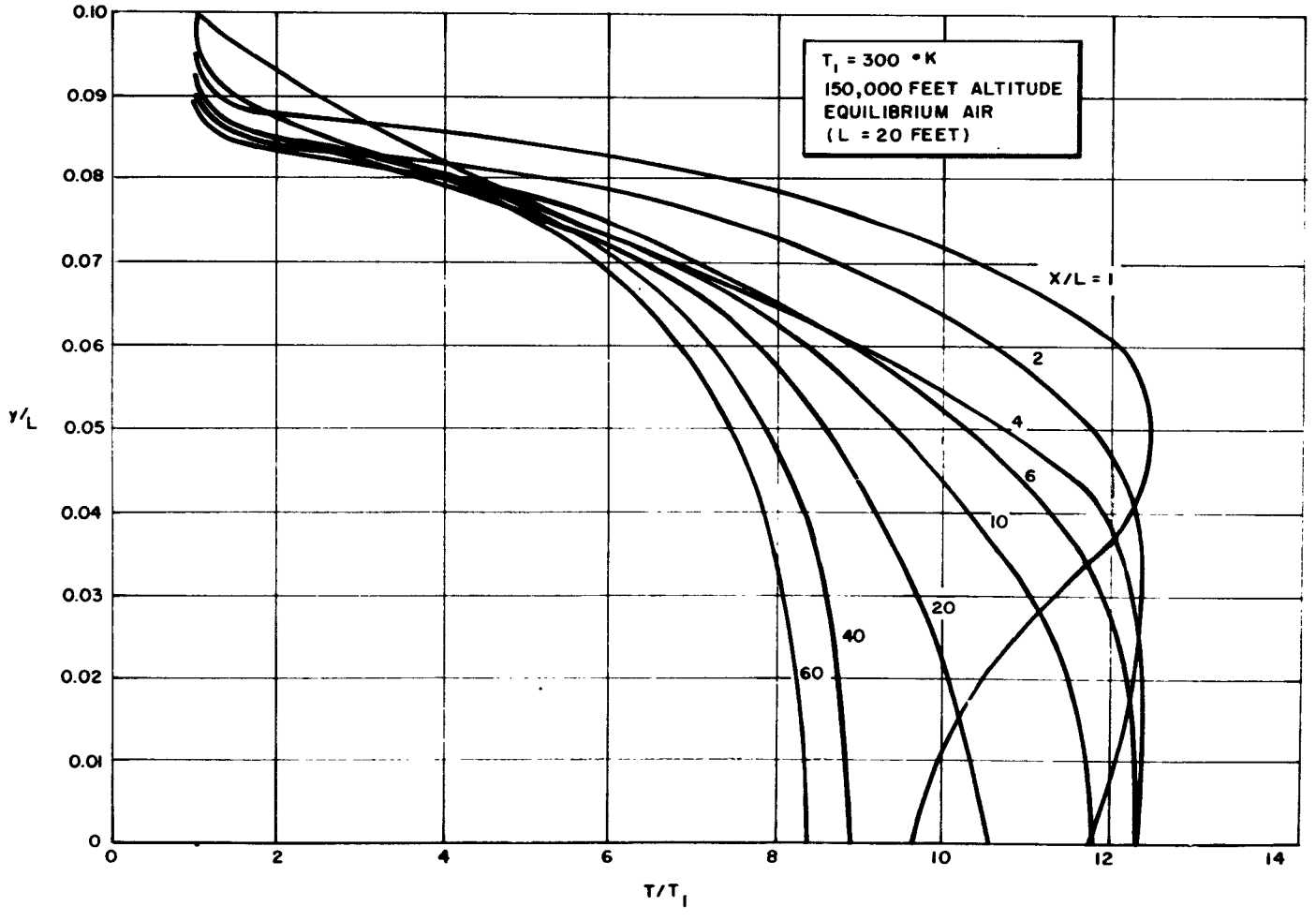

63-7570

Figure 13 TEMPERATURE PROFILES IN THE WAKE OF A 10-FOOT, 12-DEGREE CONE

V. EXPERIMENTAL STUDIES

A series of ballistic-range experiments with conical models of 10, 15, and 27-1/2-degree half angles were performed. The model velocities range between 4,000 and 17,000 ft/sec with range pressures varying from 15 to 380 mmHg in air.

The techniques for the use of a light-gas gun for launching projectiles to reentry velocities are well established. The projectile must have aerodynamic stability and must be capable of withstanding the launch loading of the gun. A conical model with a semivertex angle between 10 and 20 degrees has been developed which can withstand the launching environment of a light-gas gun to achieve velocities up to 17,000 ft/sec. This model, shown in figure 14, consists of a steel tip and titanium afterbody. It has a hollow base to provide a static margin of 15 percent. The sabot consists of an aluminum-driven disc and four Zelux petal components that interlock with the model to provide the necessary inbore support of the model during launch. Many sabot-model combinations were tried before this successful package was achieved. Failure of the model was indicated by fracture and separation of the tip or by bulging or separation at the bimetal interface. These models have a dispersion at the end of the range (approximately 40 feet from the muzzle) of about 0.75 inch. Approximately 90 percent of these models result in successful launchings. The pitch and yaw of the models, as measured from the photographic stations of the range, are generally limited to a few degrees as measured from the velocity vector.

A one-piece, steel-cone model (having a hollow base) has been used for half angles of 27.5 degrees. These models exhibit a larger dispersion than the above two-piece design.

Two 0.600-caliber light-gas-gun ranges have been used in this program.* The first range is equipped with a 12-inch diameter, double-traverse Schlieren system. The 12-inch diameter parabolic mirror is located inside a 10-foot-diameter by 14-foot-long tank. This range has been used to study the low-velocity regime (under 11,000 ft/sec) where the sensitivity of the double-traverse system is utilized for flow visualization at low density (e.g., pressures in the range $15 < P < 100$ mmHg). A 0.0005-inch Mylar foil screen has been used to provide the trigger pulse for the spark light source in the Schlieren station in some of the photographs. This screen was installed to obtain greater reliability over the light screen originally employed within the vacuum tank and to permit easy adjustment of the position of the model along its trajectory when the photograph is made. There is no effect from the foil on the flowfield since there is negligible time for any disturbance to propagate before the photograph is made.

*A more detailed description of the Avco RAD ballistics-range facility and these tests is contained in Avco RAD-TM-63-20.

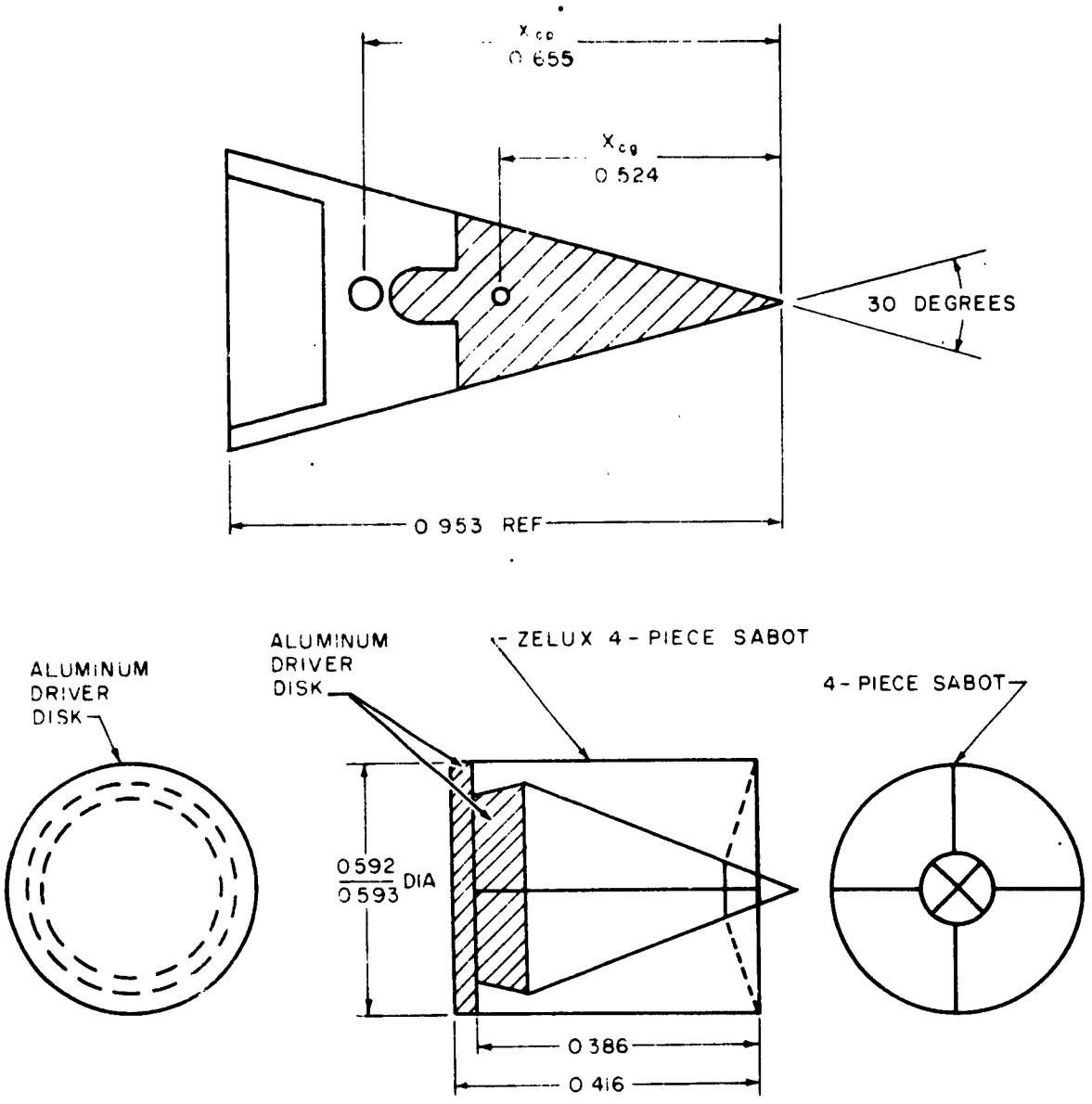

Figure 14 MODEL AND SABOT DESIGN
63-4982

A second caliber-0.600 light-gas-gun range has been used to obtain data from 11,000 to 17,000 ft/sec at pressures greater than 30 mmHg in air. Primary instrumentation on this range is a 12-inch diameter, single-pass Schlieren apparatus.

Some results covering the range of experimental conditions for which transition was clearly observable from the Schlieren photographs are compiled in table 1. Five of the Schlieren photographs which exemplify the typical features of the flowfield of a slender-body wake are presented here as figures 15, 16, 17, 18, and 19. Similar features can be seen in shadowgraph photos (e.g., figure 1, reference 5). It should be noted that the near-wake details cannot be seen in such photographs. Rather, recourse must be made to observables such as the apparent origin of the trailing shock and/or a minimum-thickness section to define the neck location.

Model pitching in the plane of the photograph is clearly identifiable by the asymmetric location of the wake within the shock layer. Small yaw angles normal to the plane of the photograph are indicated by an abnormally thick wake as compared to zero yaw at the same conditions, and by appearance of a streak down the center of the wake.

The occurrence of turbulence is always clearly identifiable for sharp bodies* and is usually preceded by an instability which manifests itself as sinusoidal waviness of the wake. Generally, the waviness is followed almost immediately followed by turbulence, but occasionally it persists for an appreciable length before breakdown into turbulence. In none of the photos are the waves observed to be opposing (i.e., peak opposite peak, valley opposite valley). Some evidence of helical motion can be seen in the cases with yaw (e.g., figure 15). By contrast, a model without yaw at approximately the same conditions is shown in figure 16. The effect of pressure on transition is demonstrated in figures 17, 18, and 19.

*This is not necessarily the case for blunt bodies, where the viscous core may be obscured by the inviscid entropy layer which enshrouds it.

TABLE I

EXPERIMENTAL CONDITIONS FOR WHICH TRANSITION IS CLEARLY OBSERVABLE FROM PHOTOGRAPHS

	Cone Semi-vertex Angle θ (degrees)	Base Diameter d (inches)	Cone Velocity V_∞ (ft/sec)	Range Pressure P_∞ (mm Hg)	M_1	$\bar{M}_1$	$(Re/ft)_1$	$Re_{x_{tr}}$
1	10	0.3	10,000	50	8.8	5.0	$4.6\ 10^6$	$2.5\ 10^6$
2	10	0.3	9,700	75	8.5	5.9	$6.9\ 10^6$	$2.7\ 10^6$
3	10	0.3	9,300	40	8.1	4.4	$3.4\ 10^6$	$9.9\ 10^5$
4	10	0.3	10,000	40	8.8	5.3	$3.7\ 10^6$	$1.7\ 10^6$
5	10	0.3	9,500	100	8.3	6.5	$8.8\ 10^6$	$2.7\ 10^6$
6	10	0.3	9,000	350	7.9	7.9	$3.0\ 10^7$	$5.5\ 10^6$
7	10	0.3	4,900	150	4.3	4.3	$6.8\ 10^6$	$1.0\ 10^6$
8	10	0.3	11,700	150	10.3	9.0	$1.7\ 10^7$	$3.6\ 10^6$
9	10	0.3	13,000	150	11.6	8.6	$1.9\ 10^7$	$6.8\ 10^6$
10	10	0.3	14,800	150	13.0	10.5	$2.1\ 10^7$	$5.6\ 10^6$
11	10	0.3	15,700	150	13.6	10.2	$2.1\ 10^7$	$1.5\ 10^7$
12	10	0.3	14,100	100	12.5	8.7	$1.4\ 10^7$	$5.3\ 10^6$
13	15	0.4	8,100	75	7.1	5.4	$5.6\ 10^6$	$2.1\ 10^6$
14	15	0.4	10,000	75	8.7	7.5	$6.7\ 10^6$	$1.7\ 10^6$
15	15	0.4	12,700	75	10.6	8.1	$7.2\ 10^6$	$2.7\ 10^6$
16	15	0.4	10,500	30	9.2	4.7	$2.9\ 10^6$	$1.7\ 10^6$
17	15	0.4	9,600	100	8.4	7.4	$8.8\ 10^6$	$2.1\ 10^6$
18	15	0.4	10,300	100	9.0	8.0	$9.6\ 10^6$	$2.2\ 10^6$
19	15	0.4	9,000	150	7.9	7.2	$1.2\ 10^7$	$2.6\ 10^6$
20	15	0.4	9,800	250	8.6	8.2	$2.3\ 10^7$	$5.1\ 10^6$
21	15	0.4	13,300	100	10.8	8.4	$8.8\ 10^6$	$3.2\ 10^6$
22	15	0.4	14,500	100	12.2	9.0	$1.1\ 10^7$	$5.6\ 10^6$
23	15	0.3	14,200	150	11.8	9.6	$1.6\ 10^7$	$3.9\ 10^6$
24	15	0.3	14,600	100	12.0	9.3	$1.0\ 10^7$	$3.7\ 10^6$
25	15	0.3	15,800	100	12.9	9.4	$1.1\ 10^7$	$4.1\ 10^6$
26	15	0.3	10,000	360	8.8	8.7	$3.3\ 10^7$	$4.3\ 10^6$
27	27-1/2	0.3	9,200	50	5.5	3.3	$1.2\ 10^6$	$3.6\ 10^5$
28	8 (NOL)	0.4	14,800	100	13.0	10.7	$1.3\ 10^7$	$6.1\ 10^6$
29	8 (NOL)	0.4	14,800	100	13.0	9.7	$1.3\ 10^7$	$9.0\ 10^6$

	ξ_{tr}	$\bar{\xi}_{tr}$	$\bar{R}e\bar{x}_{tr}$	$(Tc\ T_1)_{neck}$	$(Tc/T_1)_{tr}$
1	3.3	4.2	$1.8\ 10^6$	4.5	5.9
2	2.3	3.5	$2.8\ 10^6$	4.4	5.9
3	3.3	4.5	$1.3\ 10^6$	4.0	5.1
4	2.7	3.5	$1.3\ 10^6$	4.5	6.0
5	1.8	3.1	$3.7\ 10^6$	4.5	6.1
6	1.0	1.0	$5.5\ 10^6$	3.8	3.8
7	1.0	1.0	$1.0\ 10^6$	1.4	1.4
8	1.4	2.6	$5.8\ 10^6$	6.0	7.3
9	2.1	3.6	$8.6\ 10^6$	8.3	11.5
10	1.8	3.2	$8.3\ 10^6$	8.3	9.6
11	2.3	4.1	$7.8\ 10^6$	8.7	10.0
12	2.3	3.6	$5.8\ 10^6$	8.0	9.4
13	2.3	4.2	$2.9\ 10^6$	3.2	4.3
14	1.6	3.1	$2.8\ 10^6$	4.5	5.6
15	2.3	4.1	$3.8\ 10^6$	6.2	7.5
16	3.6	4.6	$1.1\ 10^6$	4.9	6.1
17	1.5	3.1	$3.7\ 10^6$	4.2	5.2
18	1.4	2.8	$3.8\ 10^6$	4.8	5.8
19	1.3	2.8	$5.0\ 10^6$	3.8	4.4
20	1.2	2.7	$7.9\ 10^6$	4.7	5.3
21	2.3	5.0	$5.4\ 10^6$	6.2	7.4
22	2.8	4.9	$7.4\ 10^6$	7.4	8.6
23	2.0	4.2	$6.7\ 10^6$	7.1	8.2
24	2.3	4.3	$5.3\ 10^6$	7.2	8.3
25	2.6	4.4	$5.1\ 10^6$	7.6	8.8
26	1.0	1.0	$4.3\ 10^6$	4.5	4.5
27	3.5	4.1	$2.8\ 10^5$	2.1	2.9
28	2.1	4.4	$1.0\ 10^6$	8.3	9.5
29	3.1	5.8	$1.2\ 10^6$	8.3	9.6

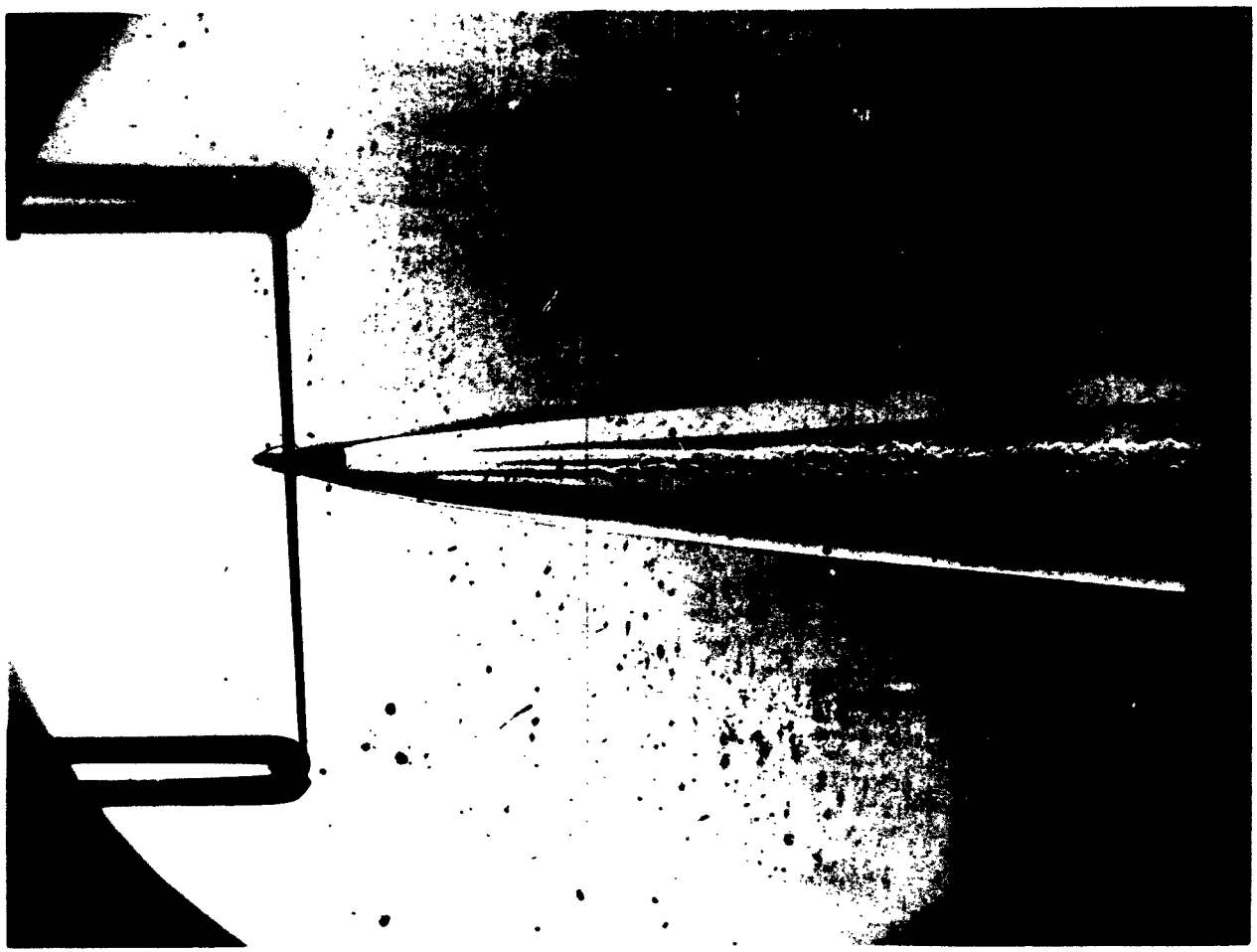

Figure 15 TYPICAL FEATURES OF A SLENDER BODY FLOW FIELD, EXAMPLE 1
10-Degree Cone V = 14,800 ft-sec
0.300-Inch Base Diameter P = 150 mm Hg

Figure 16 TYPICAL FEATURES OF A SLENDER BODY FLOW FIELD, EXAMPLE 2
10-Degree Cone V = 15,700 ft-sec
0.300-Inch Base Diameter P = 150 mm Hg

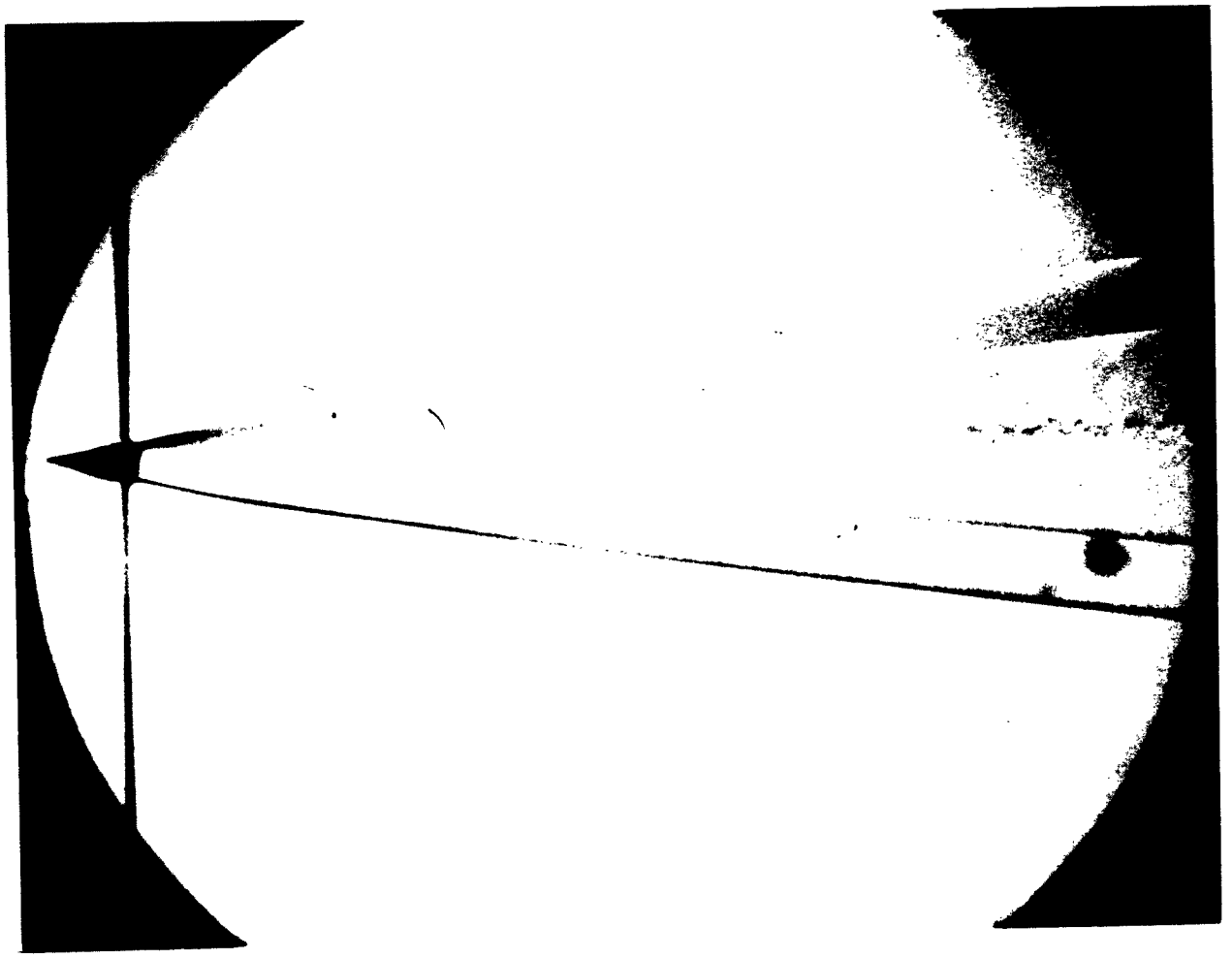

Figure 17 TYPICAL FEATURES OF A SLENDER BODY FLOW FIELD, EXAMPLE 3
10-Degree Cone V = 9,700 ft-sec
0.300-Inch Base Diameter P = 75 mm Hg

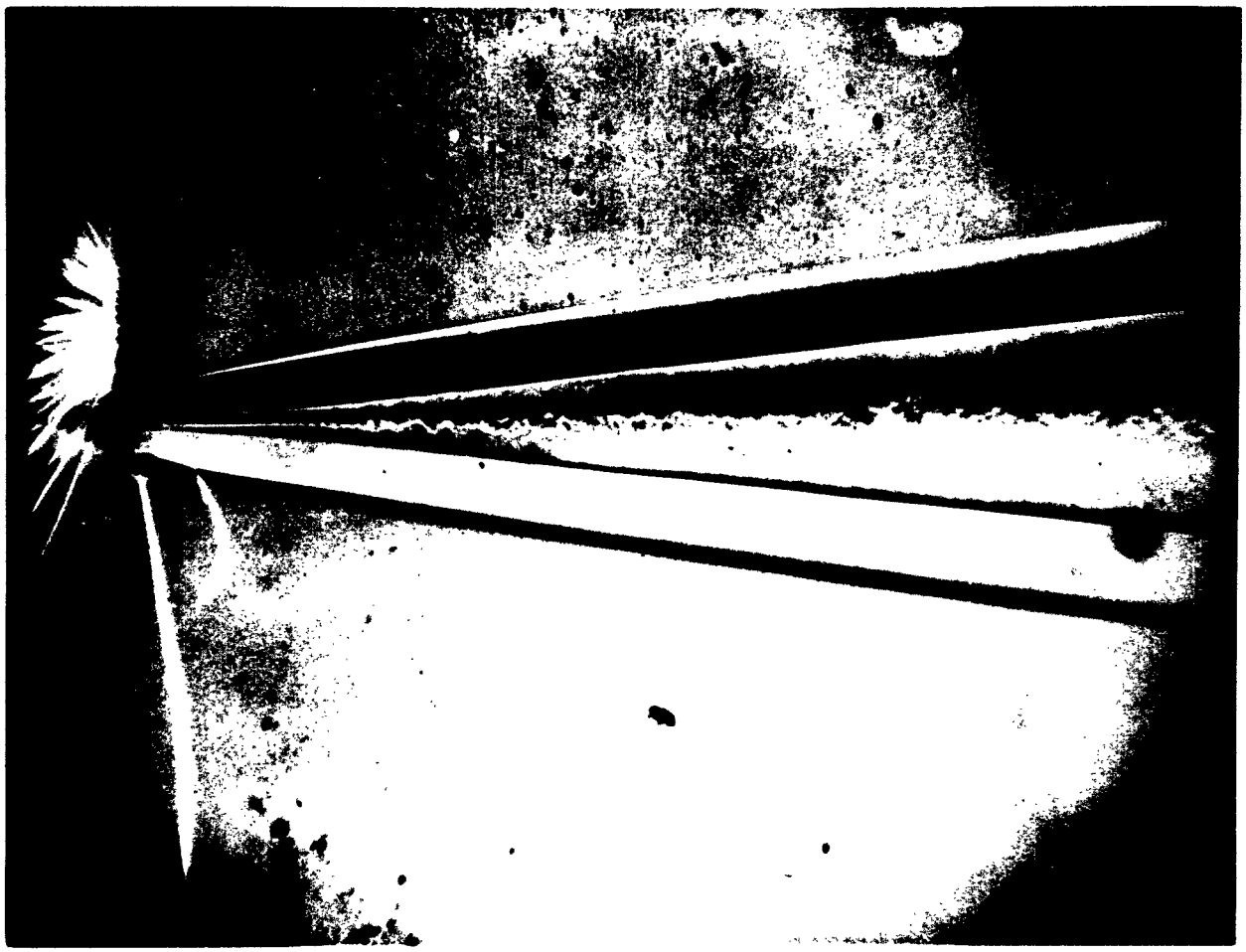

Figure 18 TYPICAL FEATURES OF A SLENDER BODY FLOW FIELD, EXAMPLE 4
15-Degree Cone V = 10,000 ft-sec
0.400-Inch Base Diameter P = 250 mm Hg

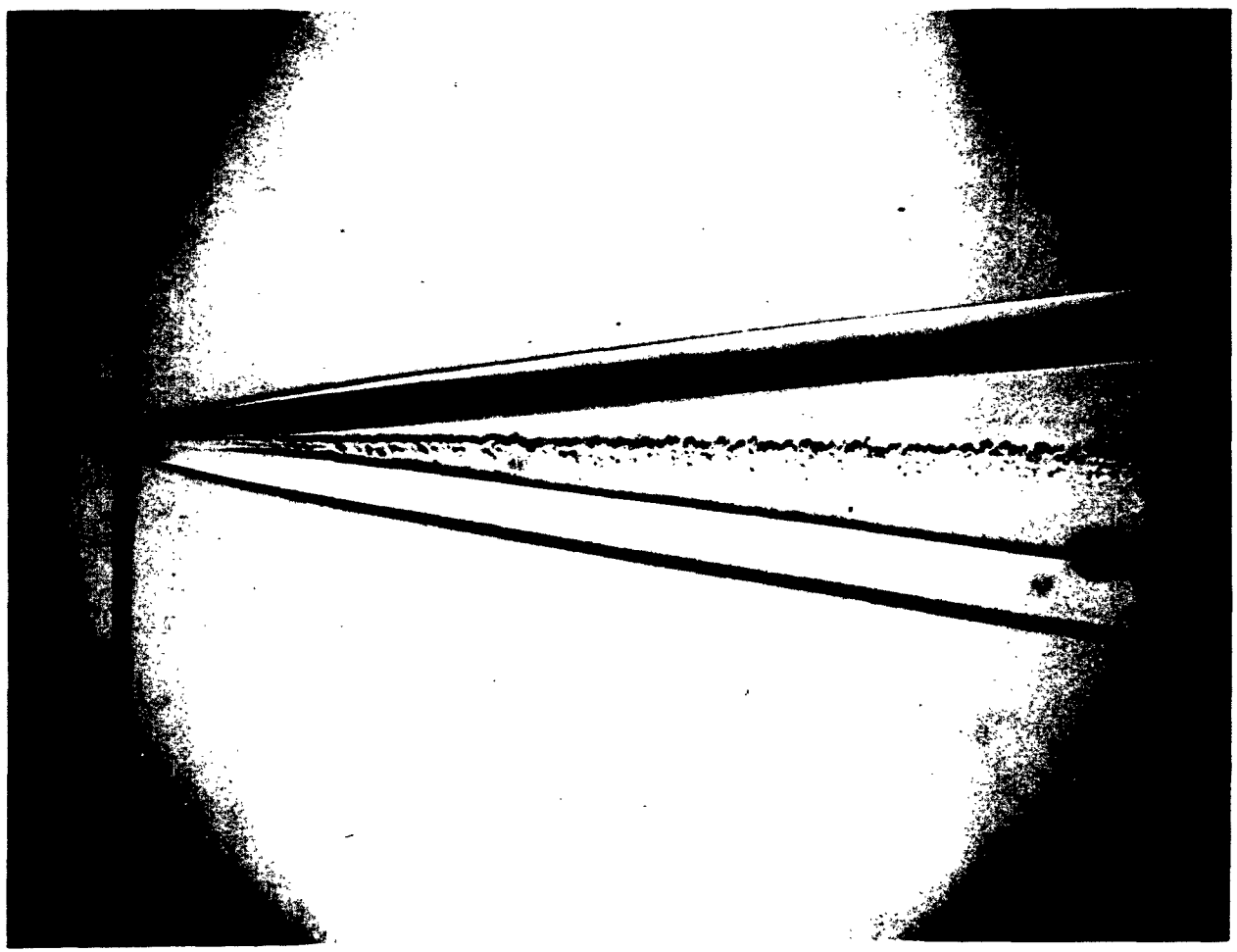

Figure 19 TYPICAL FEATURES OF A SLENDER BODY FLOW FIELD, EXAMPLE 5
10-Degree Cone V = 9,000 ft-sec
0.300-Inch Base Diameter P = 350 mm Hg

VI. TRANSITION CORRELATION

It is generally agreed that wake transition is dependent on a Reynolds number and a Mach number which are based on the relative velocity of the wake ($u_1 - u_c$), (references 4, 19, 20, and 21). Stability theory indicates that the Reynolds number and Mach number should be evaluated using physical properties at the "critical point" in the layer.* However, transition correlations commonly use properties at the outer edge of the layer and introduce a temperature ratio as a third parameter. Several length scales, namely surface distance to transition point, boundary-layer thickness, momentum thickness, etc., have been employed in defining a transition Reynolds number. None of these parameters are completely satisfactory in situations where the viscous-layer history is significant (e.g., strongly varying edge properties, nonsimilar profile shape, etc.).

Clearly, the latter remarks are appropriate to wake transition. A heuristic approach to this problem (short of a complete stability analysis) is to attempt correlation using physically reasonable length from the origin of the viscous layer to the transition point, X_{tr}, and the layer thickness at transition, δ_{tr},** both of which are readily measurable. A third possibility, however, is the relative distance***a particle travels along the axis to the transition point, $\bar{X}_{tr}$. This is a measure of the time which a disturbance which is convected with the particle has to amplify. The significance of this time is suggested by the experiments of Sato and Kuriki,[15] in which the disturbances were observed to originate at the center of the wake and grow as they convected downstream. The distance is given by:

$$\bar{X} = \int_0^t (u_1 - u_c)\, dt$$

(reference system fixed with respect to the vehicle).

A photograph of the flowfield, however, only reveals the relative distance traveled by a particle along the axis as compared with the distance traveled by the vehicle:

$$(X_{tr})_{photo} = L + \int_{t_o}^{t_1} u_c\, dt$$

---

* Gold, H., Avco RAD, Personal Communication

** δ_{tr} is defined as the wake diameter at transition.

*** i.e., in a coordinate system fixed with respect to the medium in which the body is immersed.

Therefore,

$$\bar{X}_{tr} = X_1 - \int_L^{X_1} \frac{u_c}{u_1}\, dx$$

where

$$X_1 = \int_0^{t_1} u_1\, dt$$

and

$$(X_{tr})_{photo} = L + \int_L^{X_1} \frac{u_c}{u_1}\, dx$$

The distance to transition along a wall or in a shear layer is consistent with this formulation, (i.e., with $u_c = 0$).

The preceeding analysis was used to correlate the wake-transition data from the experiments in the Avco RAD ballistics range and some from the NOL ballistics range. The Reynolds number and Mach number are defined as:

$$\overline{Re/ft}_1 = \frac{\rho_1 u_1}{\mu_1}\left(1 - \frac{u_c}{u_1}\right)$$

$$\bar{M}_1 = \frac{u_1}{a_1}\left(1 - \frac{u_c}{u_1}\right)$$

The values of $\frac{u_c}{u_1}$ and $\bar{X}_{tr}$ were computed for the experimental conditions utilizing the values of X_{tr} measured from Schlieren and shadowgraph photos. The value of δ_{tr} was also measured. (Transition was defined by the occurrence of waviness at the outer edge of the wake.) A correlation of these experimental data is offered in figures 20, 21, and 22, based on X_{tr}, δ_{tr}, and $\bar{X}_{tr}$, respectively. The scatter is at least partially due to the fact that no attempt to account for temperature effects has been included, and the ratio T_c/T_1 at transition covers a range from about 4 to 10 for the slender, high-velocity cones based

on an assumed value of $\frac{H_c}{H_1} = 0.3$ at the neck.

Some transition data of Sato and Kuriki[15] and McCarthy[16] also are included for the sake of comparison. For these data, T_c/T_1 was of the order of one. The correlation based on the measured X_{tr} shows the most scatter. The correlations based on $\bar{X}_{tr}$ and δ_{tr} have about the same scatter, although the latter has the feature of improving the correlation at low $\bar{M}_1$ (i.e., the data of references 15 and 16).

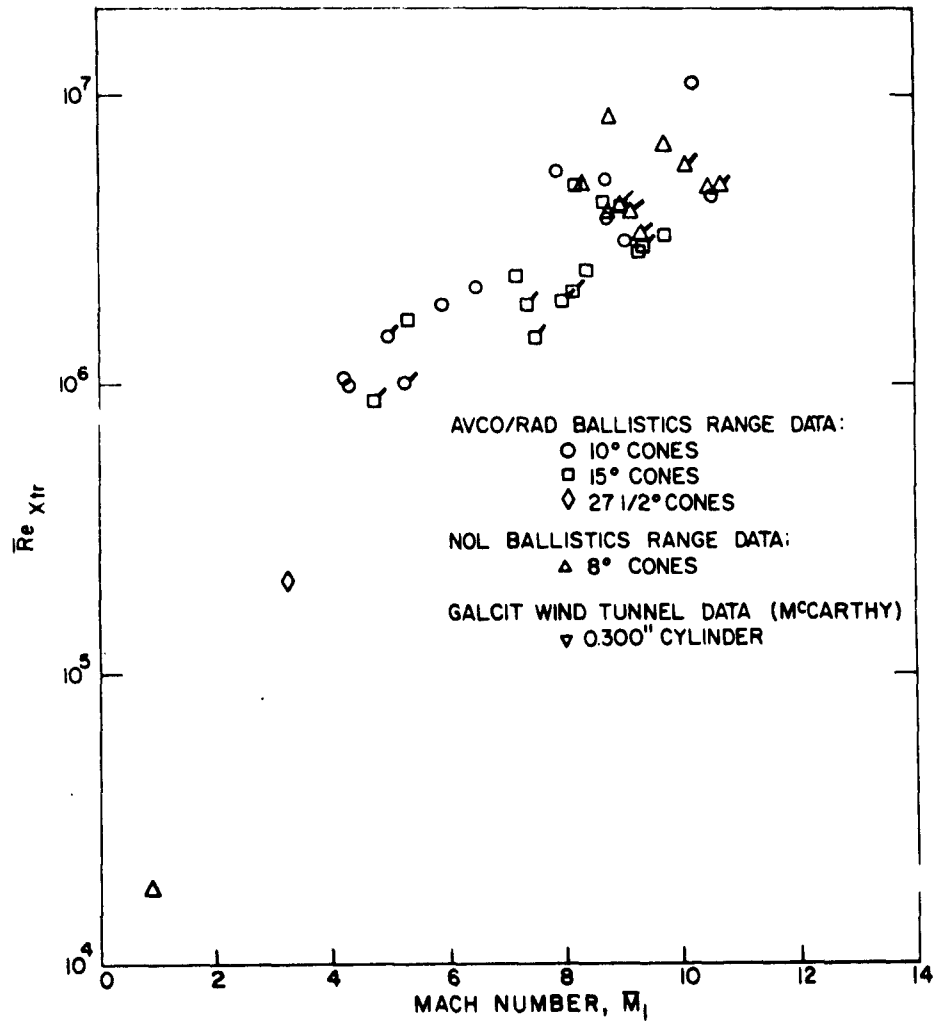

Figure 20 WAKE TRANSITION CORRELATION (BASED ON MEASURED TRANSITION DISTANCE)
63-4081

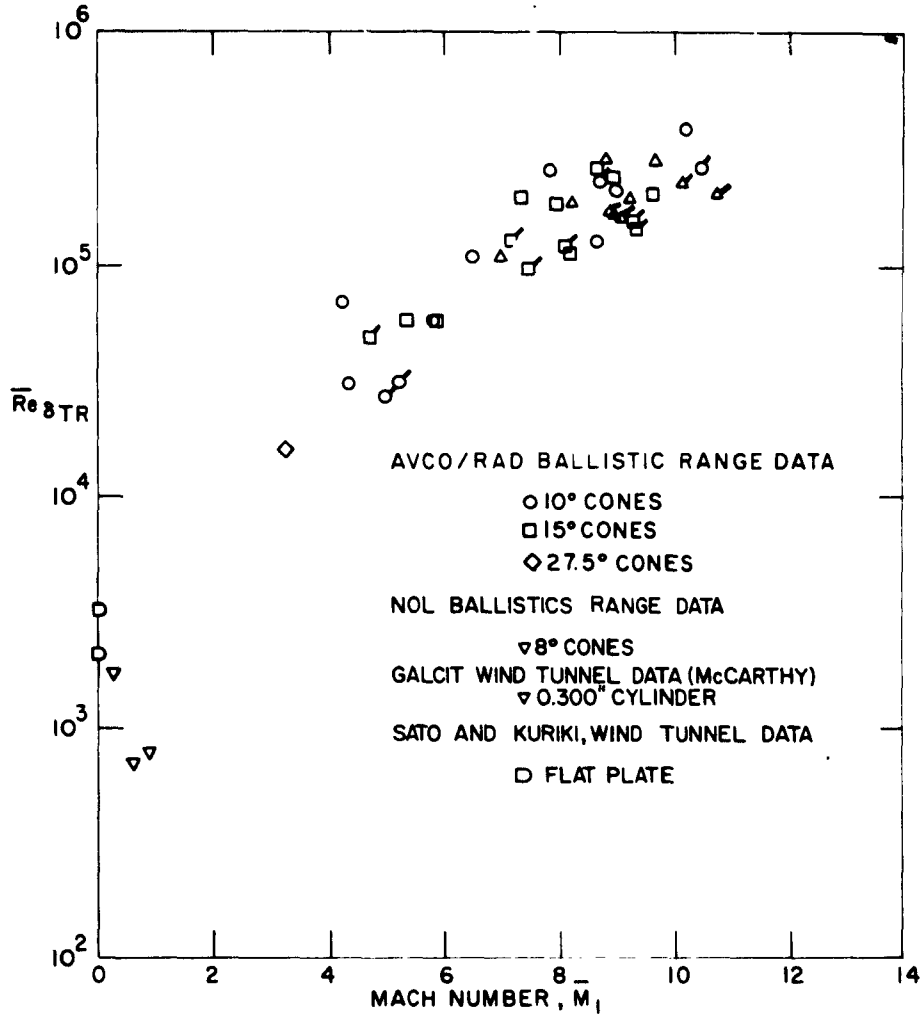

Figure 21 WAKE TRANSITION CORRELATION (BASED ON MEASURED WAKE DIAMETER)
63-4378

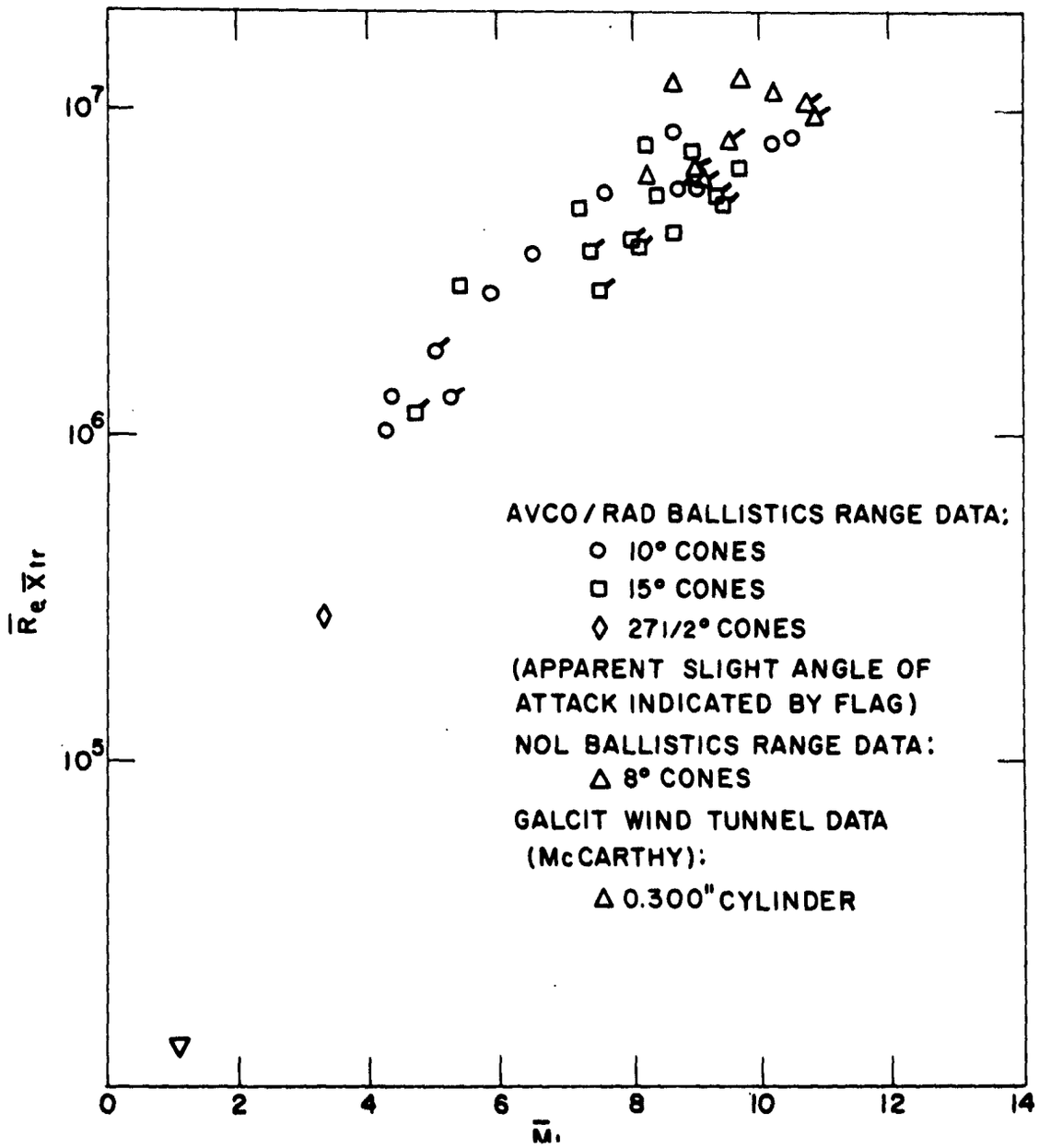

Figure 22 WAKE TRANSITION CORRELATION (BASED ON COMPUTED TRANSITION DISTANCE)
63-4078

VII. PREDICTION OF TRANSITION

The $\bar{Re}_\delta, \bar{M}_1$ and $\bar{Re}_x, \bar{M}_1$ histories of the wake of a 5-foot, 12-degree cone have been computed and are shown in figures 23 and 24. * The predicted loci of transition points is remarkably consistent for these two correlations. (Predictions on the basis of $\bar{Re}_{x_{tr}}$ indicate a long laminar wake persisting to altitudes lower than 100,000 feet). Presumably, the transition Reynolds number for the boundary layer will continue to rise with Mach number inferring that transition on the cone surface will occur in the neighborhood of 100,000 feet, at which time the near-wake and any portion of the far-wake still laminar would be tripped. **

The effect of increased vehicle size also has been investigated. As can be seen from figures 21 and 22, the transition point stays near the neck at 115,000 feet regardless of vehicle size, although as much as 300 to 400 feet of laminar run may occur behind a 15-foot cone at 200,000 feet.

The possible effects of chemical nonequilibrium on the prediction of transition for this vehicle have not been included; however, the velocity decay is only slightly affected by the temperature variation (e.g., figure 10).

It should be noted for large X the values of $\bar{Re}_x$ and $\bar{Re}_\delta$ become an inverse function of X. Hence, at some altitude above 200,000 feet, in the present example, the wake will remain completely laminar.*** This result is qualitatively consistent with conclusions reacted by Lees[4] from energy considerations.

---

* A constant velocity (22,000 ft/sec) trajectory between 200,000 and 100,000 feet is assumed.

** It is anticipated that surface ablation will have two opposing effects on the boundary-layer stability. The blowing itself tends to be destabilizing, but on the other hand it will enhance the stabilizing effects of the favorable pressure gradient (induced by viscous-inviscid interaction) by further increasing the displacement thickness.

*** This altitude bound on the occurrence of transition will, of course, depend on the size, shape, and velocity of the vehicle in question.

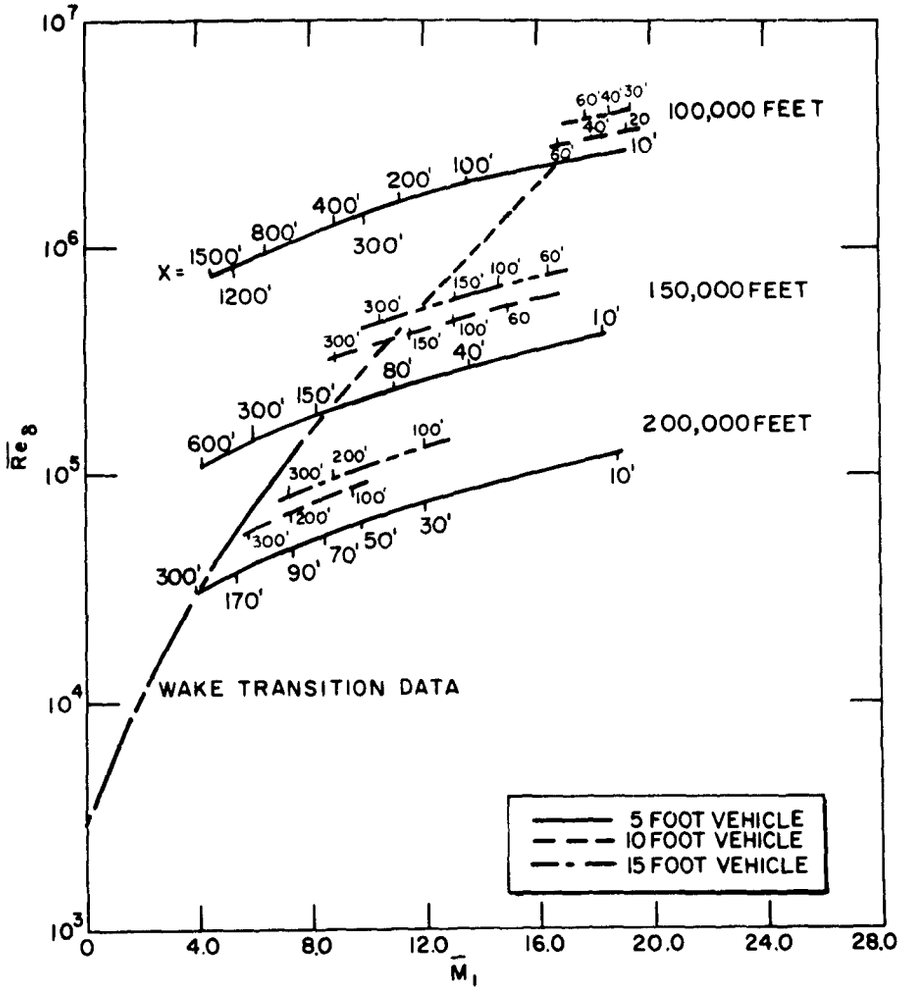

Figure 23 WAKE TRANSITION FOR A 12-DEGREE CONE AT 22,000 FT/SEC BASED ON Re_δ

63-4377

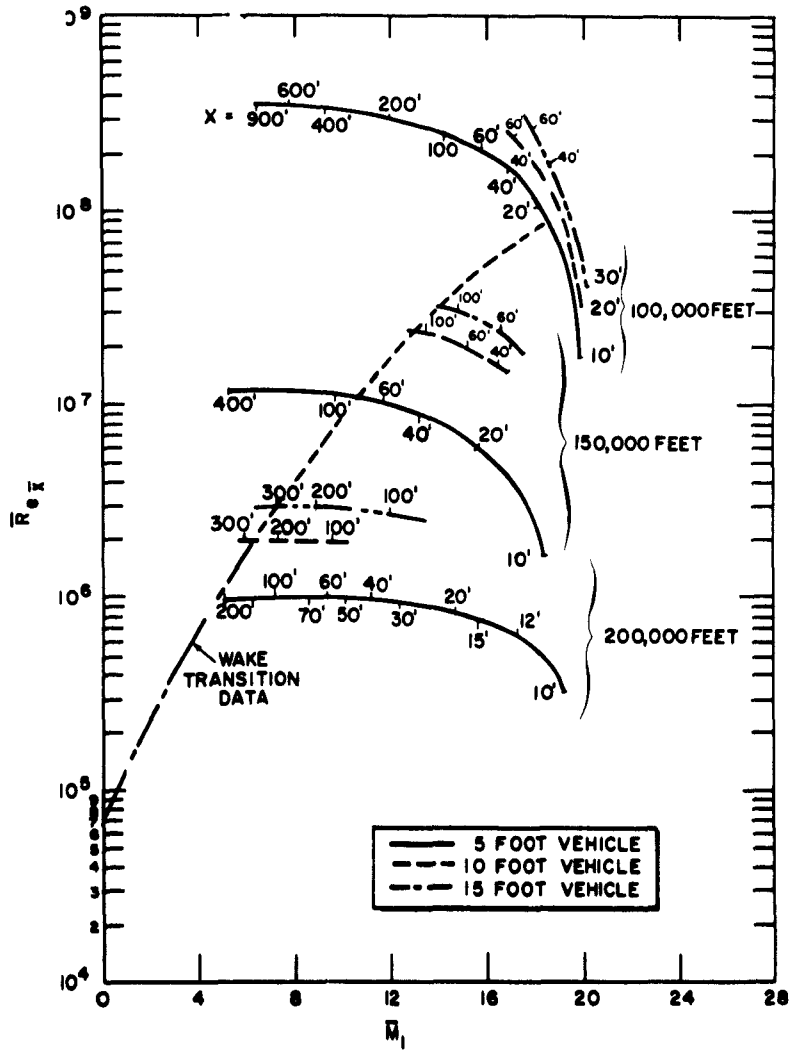

Figure 24 WAKE TRANSITION FOR A 12-DEGREE CONE AT 22,000 FT/SEC BASED ON Re_x
63-3924

VIII. NECK THICKNESS OF THE LAMINAR WAKE

As in the previous discussion (section IV) on the momentum thickness at the neck, it also may be argued that the overall wake thickness at the neck also must vary as the fourth root of Reynolds number in the axisymmetric case, as opposed to the square root in the planar (semi-infinite) case. In particular, if negligible mass addition to the viscous core in the near-wake region is assumed, then a simple mass balance yields:

$$\left[\rho_1 u_1 \delta^{j+1}\left(1 - \frac{\delta^{*j+1}}{\delta^{j+1}}\right)\right]_{neck} = \left[\rho_1 u_1 (j+1) R_b \delta \left(1 - \frac{\delta^*}{\delta}\right)\right]_{body}$$

where

$$\delta^* \equiv \left\{(j+1)\int_0^{\delta}\left(1 - \frac{\rho u}{\rho_1 u_1}\right) r^j \, dr\right\}^{1/j+1}$$

For a cone this can be reduced to

$$\left[\frac{\delta}{d}(Re_d)^{1/4}\right]_{neck} = \left[\frac{(\rho_1 u_1 \mu_1)_{cone}}{(\rho_1 u_1 \mu_1)_{neck}}\left(\frac{1}{2 \sin \theta}\right)\right]^{1/4} f(M_\infty, \theta, T_w)$$

$$\approx \left[\frac{P_{cone}/P_\infty}{2 \sin \theta}\right]^{1/4} f(M_\infty, \theta, T_w) .$$

$$\approx \left[\frac{\gamma}{2} M_\infty\right]^{1/4} f[M_\infty, \theta, T_w]$$

where

$$f\ (M_\infty,\ \theta,\ T_w) = \left\{ \frac{\left[\left(\frac{\delta}{L}\ \sqrt{Re_L}\right)\left(1 - \frac{\delta^*}{\delta}\right)\right]_{cone}}{\left[1 - \left(\frac{\delta^*}{\delta}\right)^2\right]_{neck}} \right\}^{1/2}$$

The parameter $\left[\frac{\delta}{d}\ (Re_d)^{1/4}\right]_{neck}$ was found to be essentially a function solely of Mach number for the range of cone-angle and Mach-number combinations encountered in the present tests, when computed in the manner discussed in in the previous section on initial conditions (i. e., employing the values of δ which give the proper drag at the neck when used with the assumed separation-point velocity profile). The values of this parameter based on the experimentally measured neck thickness are shown in figure 25 to compare remarkably well with the computed curve. *

*The thickness δ in this figure is the wake diameter rather than radius.

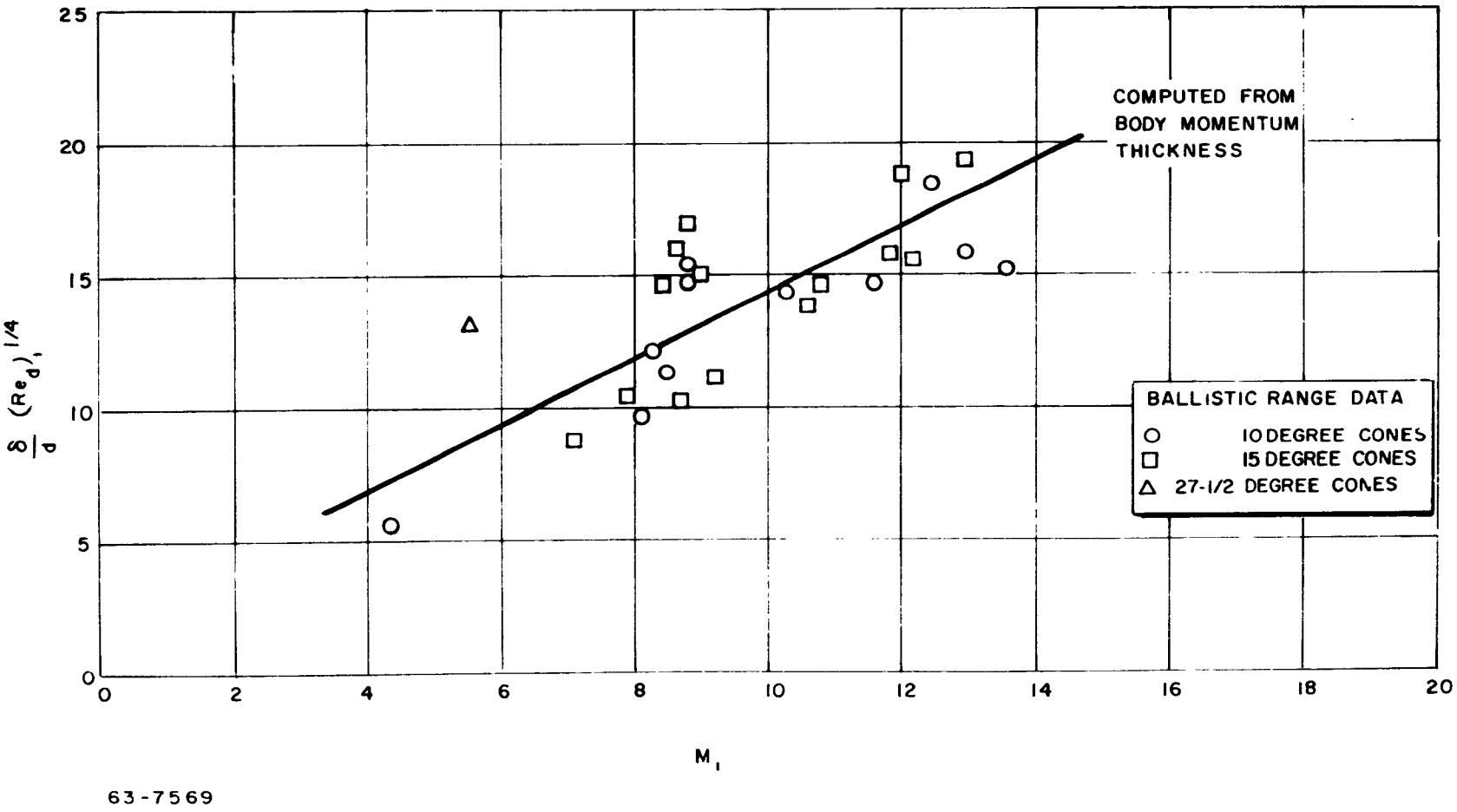

Figure 25 LAMINAR WAKE THICKNESS AT THE NECK FOR SHARP CONES

IX. CONCLUSIONS

The results of theoretical and experimental investigations of the flow in the wake of slender hypersonic vehicles have been presented. In particular, nonsimilar solution of the governing equations is contrasted with similar and Karman-Pohlhausen-type solutions. The similar solution is shown to be inadequate near the neck of the wake of a slender body, although correct asymptotically at large distances. The Karman-Pohlhausen technique appears to offer a good compromise between simplicity and accuracy for slender-body wakes. Some numerical examples for slender and blunt bodies are presented using the nonsimilar solution.

The results of a series of ballistic range experiments on slender cones in the Avco RAD facilities are summarized and discussed. The preceding analysis is used to compute appropriate parameters for the correlation of wake transition and neck diameter from these data. Moreover, predictions of wake transition for a 5-foot, 12-degree half-angle cone at 22,000 ft/sec are made, which indicate transition moves from about 250 feet behind the cone apex at an altitude of 200,000 feet to about 20 feet at 100,000 feet. Increasing the cone length to 15 feet is shown to add about 100 feet to the length of the laminar trail at 200,000 feet, and to add about 15 feet at 100,000 feet. The existence of an altitude above which transition cannot occur (for a vehicle of given size and velocity) also is indicated by the correlation.

X. REFERENCES

1. Feldman, S., On Trails of Axisymmetric Hypersonic Blunt Bodies Flying Through the Atmosphere, J. Aerospace Sci. 28 (6) (June 1961) pp. 433-448.

2. Lees, L. and L. Hromas, Turbulent Diffusion in the Wake of a Blunt-Nosed Body at Hypersonic Speeds, J. Aerospace Sci. 29 (8) (August 1962) pp. 976-993.

3. Vaglio-Laurin, R. and M. Bloom, Chemical Effects in External Hypersonic Flows, Progress in Astronautics and Rocketry, Vol. 7, Hypersonic Flow Research, Academic Press, New York (1962) pp. 205-254.

4. Lees, L., Hypersonic Wakes and Trails (ARS Preprint 2662-62), Presented at 17th Annual Meeting of the ARS (13-18 November 1962).

5. Vaglio-Laurin, R., M.H. Bloom and R. W. Byrne, Aerophysical Aspects of Slender Body Re-entry, (ARS Preprint 2674-62), Presented at 17th Annual Meeting of the ARS, (13-18 November 1962).

6. Goldstein, S., Modern Developments in Fluid Dynamics, Oxford Univ. Press, London (1938); Schlicting, H., Boundary Layer Theory, McGraw-Hill, New York (1955).

7. Pallone, A., Nonsimilar Solutions of the Compressible Laminar Boundary Layer Equations with Applications to the Upstream-Transpiration Problem, J. Aerospace Sci. 28 (6) pp. 450-456.

8. Bloom, M.H. and M.H. Steiger, Diffusion and Chemical Relaxation in Free Mixing, (IAS Paper No. 63-67), Presented at IAS 31st Annual Meeting, (21-23 January 1953).

9. Lien, H., J. Erdos and A. Pallone, Nonequilibrium Wakes with Laminar and Turbulent Transport, Presented at AIAA Conference on Physics of Entry into Planetary Atmospheres, M.I.T., August 26-28, 1963, (Preprint No. 63-447).

10. Pallone, A., J. Moore and J. Erdos, Nonequilibrium, Nonsimilar Solutions of the Laminar Boundary Layer Equations, Avco RAD-TM-63-58, August 1963.

11. Denison, M.R. and E. Baum, Compressible Free Shear Layer with Finite Initial Thickness, (IAS Paper No. 62-125), Presented at IAS National Summer Meeting (19 to 22 June 1962).

12. Chapman, D. R., D. M. Kuehn and H. K. Larson, Investigation of Separated Flows in Supersonic and Subsonic Streams with Emphasis on the Effect of Transition, NACA Report 1356 (1958).

13. Cohen, C. and E. Reshotko, Similar Solutions for the Compressible Laminar Boundary Layer with Heat Transfer and Pressure Gradient, NACA Technical Note 3325 (February 1955).

14. Gaffney, H., Polynomial Curve Fits of the Mollier Diagram for Air in Chemical Equilibrium, Avco RAD (Report to Be Published).

15. Sato, H. and K. Kuriki, The Mechanism of Transition in the Wake of a Thin Flat Plate Placed Parallel to a Uniform Flow, Journal of Fluid Mechanics, 11. No. 3 (November 1961).

16. McCarthy, J. F., Hypersonic Wakes, GALCIT Hypersonic Research Project Memorandum No. 67 (July 1962).

17. Czarnecki, K., and M. Jackson, Effects of Nose Angle and Mach Number on Transition on Cones at Supersonic Speeds, NACA TN 4388 (September 1958).

18. Schueler, C., A. Comparison of Transition Reynolds Numbers from 12 and 40-inch Supersonic Tunnels, AEDC-TDR-63-57 (March 1963).

19. Webb, W., L. Hromas, and L. Lees, Hypersonic Wake Transition, AIAA Journal, 1, 3 (March 1963) pp. 719-721.

20. Lin, C. C., Theory of Hydrodynamic Stability, Cambridge Monographs on Mechanics and Applied Mathematics, Cambridge Univ. Press (1955).

21. Pai, S., On the Stability of Two-Dimensional Laminar Jet Flow of Gas, J. Aeron. Sci., 18 (1951) pp. 731-742.

DISTRIBUTION

Addressee	No. of Copies
AFBSD, Attn: BSYDF, Lt. K. Jefferson	2
AFBSD, Attn: BSTRA	1
AFSSD AF Unit Post Office Los Angeles, California Attn: Capt. Lewis, SSTRE	1
Aerospace Corporation San Bernardino, California Attn: H. Claflin	30
ARPA Washington, 25, D.C., Attn: C.E. McLain	1
ARPA Washington, 26, D.C. Attn: Lt. Col. McNamee	1
ASD Wright-Patterson AFB, Ohio Attn: D.L. Schmidt, ASRNC-2	1
AFCRL L.G. Hanscom Field Bedford, Massachusetts Attn: N. W. Rosenberg, CRZAC	1
SAC (DORQ) Offutt AFB, Nebraska	1
AMC (ORDAB-HT) Redstone Arsenal Huntsville, Alabama	1
ATIC (AFCIN-4BLA) Wright-Patterson AFB, Ohio	1
AUL Maxwell AFB, Alabama	1
Chief, DASA Washington 25, D.C.	1
NASA, Ames Research Center Moffett Field, California	1
NASA, Lewis Research Center Cleveland, Ohio	1
NASA, Langley Research Center Virginia	1
Department of the Navy Washington, D.C. Attn: SP-272	1

DISTRIBUTION (Cont'd)

Addressee	No. of Copies
Central Intelligence Agency Washington, D. C. Attn: OCR-Std	2
BAMIRAC, University of Michigan Ann Arbor, Michigan Attn: R. Nichols	1
Batelle Memorial Institute Columbus, Ohio	1
Bendix Systems Division Ann Arbor, Michigan Attn: M. Katz	1
General Applied Science Laboratory Attn: M. Bloom	1
General Electric Company 3198 Chestnut Street Philadelphia, Pennsylvania	1
Hughes Aircraft Company Culver City, California Attn: E. Chrisler	1
Kaman Nuclear Garden of the Gods Road Colorado Springs, Colorado Attn: A. P. Bridges	1
Lincoln Laboratory, M.I.T. Lexington 73, Massachusetts Attn: F. McNamara	1
Los Alamos Scientific Laboratory Los Alamos, New Mexico	1
The RAND Corporation Santa Monica, California Attn: C. Gazley	1
UCRL, "A" Division Livermore, California	1
Defense Documentation Center Arlington Hall Station Arlington 12, Virginia	10
Lincoln Laboratory, M.I.T. Lexington, Massachusetts Attn: V. A. Nedzel	1

DISTRIBUTION (Concl'd)

Addressee	No. of Copies
Lincoln Laboratory, M.I.T. P.O. Box 4188 Norton Air Force Base, California Attn: J. Vernon	1
Central Files	1
Document Control	5
Research Library	97

DDC-

A series of ballistic-range experiments with conical models of 10, 15, and 27-1/2-degree half-angles are described. The model velocity ranges between 4,000 and 17,000 ft/sec with range pressures varying from 15 to 380 mmHg in air. The experimental data is discussed in detail, and the analysis is used to compute and correlate appropriate transition parameters.

Based on the correlation, predictions of the location of transition in the wake of a 12-degree half-angle cone at 22,000 ft/sec are made for the altitude range from 200,000 to 100,000 feet. For example, transition is placed at approximately 250, 100, and 20 feet from the apex of a 5-foot cone at altitudes of 200,000, 150,000 and 100,000 feet, respectively, assuming the boundary layer on the cone surface remains laminar.

UNCLASSIFIED

DDC-

A series of ballistic-range experiments with conical models of 10, 15, and 27-1/2-degree half-angles are described. The model velocity ranges between 4,000 and 17,000 ft/sec with range pressures varying from 15 to 380 mmHg in air. The experimental data is discussed in detail, and the analysis is used to compute and correlate appropriate transition parameters.

Based on the correlation, predictions of the location of transition in the wake of a 12-degree half-angle cone at 22,000 ft/sec are made for the altitude range from 200,000 to 100,000 feet. For example, transition is placed at approximately 250, 100, and 20 feet from the apex of a 5-foot cone at altitudes of 200,000, 150,000 and 100,000 feet, respectively, assuming the boundary layer on the cone surface remains laminar.

UNCLASSIFIED

UNCLASSIFIED

DDC-

Avco Corporation, Research and Advanced Development Division, Wilmington, Massachusetts. HYPERSONIC LAMINAR WAKES AND TRANSITION STUDIES, by A. J. Pallone, J. I. Erdos, and J. Eckerman, 25 November 1963. 70pp.incl. illus. (Technical Memorandum TR-63-33, Rev. 1) Contract No. AF04(694)-239. Tasks 3.1 and 3.5 -- REST Project.

Unclassified report

This report presents the results of theoretical and experimental investigations of the flow in the wake of hypersonic vehicles. Nonsimilar solutions of the equations governing the "far wake" are obtained and contrasted with similar solutions and with solutions involving the Karman-Pohlhausen approach. Numerical examples of the flow field in the wake of ballistic-range and wind-tunnel models and of a flight-size vehicle are presented.

(over)

UNCLASSIFIED

1. Fluid flow
2. Hypersonic flow
3. Trails-hypersonic vehicle
4. Wake
- I. Pallone, A. J.
- II. Erdos, J. I.
- III. Eckerman, J.
- IV. Avco, Research and Advanced Development Division
- V. Contract AF04(694)-239
- VI. Series
- VII. Title

UNCLASSIFIED

DDC-

Avco Corporation, Research and Advanced Development Division, Wilmington, Massachusetts. HYPERSONIC LAMINAR WAKES AND TRANSITION STUDIES, by A. J. Pallone, J. I. Erdos, and J. Eckerman, 25 November 1963. 70pp.incl. illus. (Technical Memorandum TR-63-33, Rev. 1) Contract No. AF04(694)-239. Tasks 3.1 and 3.5 -- REST Project.

Unclassified report

This report presents the results of theoretical and experimental investigations of the flow in the wake of hypersonic vehicles. Nonsimilar solutions of the equations governing the "far wake" are obtained and contrasted with similar solutions and with solutions involving the Karman-Pohlhausen approach. Numerical examples of the flow field in the wake of ballistic-range and wind-tunnel models and of a flight-size vehicle are presented.

(over)

UNCLASSIFIED

1. Fluid flow
2. Hypersonic flow
3. Trails-hypersonic vehicle
4. Wake
- I. Pallone, A. J.
- II. Erdos, J. I.
- III. Eckerman, J.
- IV. Avco, Research and Advanced Development Division
- V. Contract AF04(694)-239
- VI. Series
- VII. Title

UNCLASSIFIED